# Synthesis of minerals

**Balitsky V.S.[1], Balitsky D.V.[2], Balitskaya L.V.[1], Setkova T.V.[1], Bublikova T.M.[1]**
**Crystal growth of quartz-like gallium orthophosphate by refluxed hydrothermal method** UDC 549.057

*[1]IEM RAS, Chernogolovka* (balvlad@iem.ac.ru), *[2] Denevr, France*

**Abstract.** The homogeneous single crystals of a quartz-like gallium orthophosphate (α-$GaPO_4$) weighing up to 30 grams on seeds of various crystallographic orientations using the previously developed hydrothermal evaporation-recirculating method of crystal growth was first carried out. Crystal growth was performed in aqueous solutions of mixtures of hydrochloric, orthophosphoric (or sulfuric) acids at temperatures of 150–260 °C and pressures of saturated steam (4–5 MPa). Under certain conditions, crystal growth rates reach 1.0 mm/day. Despite the relatively low temperatures and pressures, the crystals do not contain molecular water. Although hydroxyl group OH is present in crystals but in very limited quantities.

***Keywords**: crystal growth, gallium orthophosphate, quartz, epitaxial growth, piezoelectric*

Gallium orthophosphate crystals with a quartz structure ($\alpha$-$GaPO_4$) are the most attractive among the whole family of quartz-like materials: in addition to high piezoelectric characteristics, they have a unique (up to 933 °C) temperature stability of the quartz-like structure. Typically, $\alpha$-$GaPO_4$ crystals are grown from concentrated (6 - 15 M) solutions of orthophosphoric and sulfuric acids or their mixtures by the method of gradual temperature increase from 150 to 260 °C (Demianets, 2001; Yot et al., 2001) or by flux method with slow from 950 to 600 °C (Armand et al., 2008).

In the present work, the growth of α-$GaPO_4$ crystals was carried out by the hydrothermal refluxed method. This method we successfully used to grow $\alpha$-$GeO_2$ crystals (Balitsky et al., 1997; Balitsky et al., 2019). Since $\alpha$-$GaPO_4$, in contrast to metastable germanium oxide is in the stability region of the quartz-like (trigonal) structure up to 933 °C, it was possible to raise the crystal growth temperature to 260 °C. The experiments were performed in special crystallizers made of 1X18H9T stainless steel. Crystallizers were protected from acid corrosion by contact-type linings made of heat-resistant (up to 260 - 280 °C) fluoroplastic (PTFE).

The $\alpha$-$GaPO_4$ crystals were grown on their own seeds and epitaxially on quartz substrates. Crystalline gallium orthophosphate was used as a nutrient. The retrograde solubility of $\alpha$-$GaPO_4$ in concentrated solutions of phosphoric and sulfuric acids below the temperature of 335 °C complicated the procedure for preparing and conducting experiments on the crystal growth using the refluxed method. The seeds from $\alpha$-$GaPO_4$ crystals can dissolve already when preparing the crystallizer for the experiment. In addition, the use of fluoroplastic linings does not allow the growth of crystals at temperatures above 260 °C. In this regard, the use of quartz substrates for epitaxial growth of $\alpha$-$GaPO_4$ crystals is of particular importance, since quartz is practically insoluble in solutions of phosphoric and sulfuric acids.

Crystal growth was occurred on seed plates of various crystallographic orientations cut out of $\alpha$-$GaPO_4$ crystals and synthetic quartz. Seeds were located in the lower, hotter growth chamber. A perforated basket with small fragments of $\alpha$-$GaPO_4$ nutrient (up to 3–5 mm in diameter) was placed above this chamber. In the central part of the basket with nutrient has a hole for the steam escape from the lower growth chamber to the refrigerator located directly above the nutrient. Directing devices of the refrigerator for condensate drain are arranged in such a way that a large proportion of condensate flows directly into the chamber with nutrient and dissolving it. The walls of the bottom part of the chamber have holes with a diameter of 1–1.5 mm through which a saturated solution flows into the lower chamber of the crystallizer their suspended seeds placed.

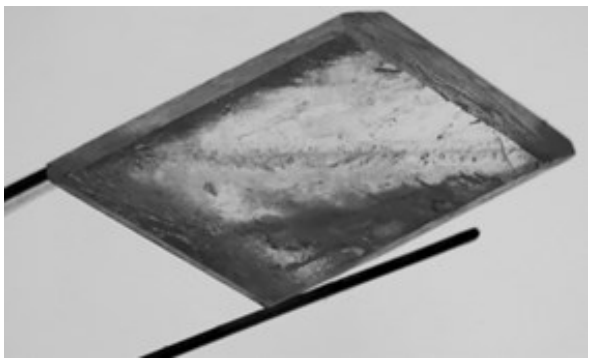

**Fig. 1.** $\alpha$-$GaPO_4$ crystal grown on a ZY seed.

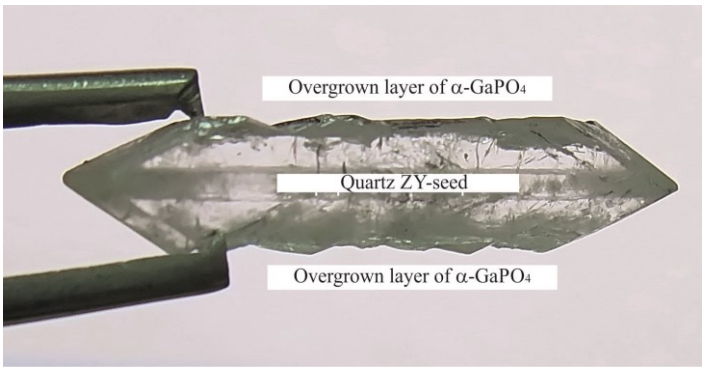


**Fig. 2**. Epitaxial growth of $\alpha$-$GaPO_4$ on a single crystal quartz ZY - seed.

As a result, supersaturation occurs in the lower growth chamber leading to the nucleation and crystal growth of $\alpha$-$GaPO_4$ (Fig. 1,2). The process takes place until nutrient complete exhaustion. The growth rate of $\alpha$-$GaPO_4$ crystals on a quartz seed reaches 1.0 mm/day under certain conditions (Fig. 2). Epitaxial growth of another structural analogue of quartz (aluminum orthophosphate) on a quartz substrate was realized earlier, but by a method of gradual temperature increase in the area of its retrograde solubility (Motchany and Chvanski, 2001). Despite the relatively low temperatures and pressures, the crystals grown in sulfuric acid solutions do not contain molecular water. The hydroxyl group OH present in very limited quantities.

Thus, the homogeneous single crystals of quartz-like gallium orthophosphate ($\alpha$-$GaPO_4$) were grown for the first time on seeds (including quartz) of different crystallographic orientations using the previously developed hydrothermal refluxed method of crystal growth. Crystal growth was performed in aqueous solutions of mixtures of hydrochloric, phosphoric or sulfuric acids at temperatures of 150–260 °C and pressures of saturated steam (3–5 MPa). The crystal growth rates reach 1.0 mm/day under certain conditions. The crystals do not contain molecular water and have a hydroxyl group OH in small amounts.

The reported study was funded by RFBR, project number 17-05-00976.

**References:**

Armand P., Beaurain M., Ruffle B., Menaert B., Balitsky D., Clement S., Papet P. (2008) Characterizations of piezoelectric $GaPO_4$ single crystals grown by the flux method. Journal of Crystal Growth. 310, 1455–1459.

Demianets L.N. (2001) Gallium orthophosphate hydrothermal growth at high temperatures (320 °C). Annales de Chimie Science des Matériaux. 26, 1, 67–74.

Balitsky D.V., Balitsky V.S., Puscharovsky D.Yu., KosenkoA.V., Bondarenko G.V. (1997) Growth and characterization of the $GeO_2$ single crystals with quartz structure. Journal of Crystal Growth. 180, 212–219.

Balitsky V. S., Balitsky D. V., Pushcharovsky D. Yu., Balitskaya L. V., Setkova T. V., and Dokina T. N. (2019) Epitaxial growth, morphology, and temperature stability of quartz-like germanium dioxide crystals Doklady Earth Sciences. 485, 1, 264–267.

Yot P., Cambon O., Balitsky D., Goiffon A., Philippot E. Capelle B., Detaint J. (2001) Advances in crystal growth and characterizations of gallium orthophosphate, $GaPO_4$. Journal of Crystal Growth, 224, 294–302.

Motchany A.I. and Chvanski P.P. (2001) Crystal growth of an α-quartz like piezoelectric material, berlinite. Ann. Chim.Sci.Mat. 26, 199-208.

## Balitsky V.S.[1], Balitskaya L.V.[1], Pushcharovsky D.Yu.[2], Setkova T.V.[1], Kvas P.S.[1,2], Nekrasov A.N.[1], Bublikova T.M.[1], Nesterova V.A.[1,2](Ga-, Ge) - containing topaz single crystals: growth, morphology and gallium and germanium distribution UDC 549.612

[1] IEM RAS, Chernogolovka, [2] Department of Geology, Lomonosov MSU, Moscow (balvlad@iem.ac.ru)

**Abstract.** Single crystals growth of topaz doped with gallium and germanium was carried out for the first time. The crystals were grown by the hydrothermal method of temperature difference using fluoride solutions at a temperature of 600–650 °C and a pressure of 100 MPa. Overgrown layer of (Ga, Ge) -containing topaz with a thickness of up to 4 mm on one side of the seed was obtained. EMPA has shown the highly uneven distribution of gallium and germanium in overgrown layer. The maximum replacement of silicon and aluminum by the indicated elements occurs at the boundary of the seed crystal and the overgrown layer, reaching 25 wt.% $GeO_2$ and 6 wt.% $Ga_2O_3$, respectively.

***Keywords:*** *topaz, crystal growth, hydrothermal synthesis, gallium, germanium*

**Introduction.** Crystal growth of topaz is very interesting not only because using in jewelry industry, but also because of the possibility of using topaz crystals with doped components (Ga, Ge) as a new functional materials. Interest in gallium and germanium replaced topaz crystal is also founded by the general problem of Ge and Ga isomorphism in aluminosilicate minerals. It is known that gallium and germanium are similar in chemical properties to aluminum and silicon, respectively, but the size of the ions $Ga^{3+}$ and $Ge^{4+}$ is bigger ($rGe^{4+}/rSi^{4+}$=2.04; $rGa^{3+}/rAl^{3+}$=1.17). The chemical deformations that can occur in the topaz structure with entering larger Ga and Ge cations may be equivalent to changes under high pressure (Gatta et al., 2014). Accordingly, such crystals may show new physical properties. Previously B. Wunder (Wunder, 1997) synthesized the germanium analogue of topaz at high thermobaric parameters (temperature 650 °C and pressure 2 GPa). Later the Ge-analogue of topaz was discovered at the Tsumeb deposit, Namibia (Schlüter et al. 2010) and was added in the IMA-CNMNC as a new mineral krieselite. At the same time, Ga-containing topaz was not founded in nature and was not synthesized in laboratory. This article presents the first results on the crystallization of Ga,Ge-containing topaz.

**Experimental methods.** Crystal growth was carried out by hydrothermal method of temperature difference according to the method developed earlier (Balitsky et al., 2002) using high-temperature autoclaves with a volume of 280 ml made of Cr-Ni alloy. Autoclaves were placed in a group of electrical furnace with two-section heaters. The duration of the

experiments was 30-60 days. Crystals were grown at temperatures from 500 to 780 °C, pressures from 20 to 180 MPa. The pressure was set by the density of the fluid in the autoclave and evaluated by P-V-T diagram for pure water (Naumov and others, 1971). Temperature controlled by standard thermal measuring device (Thermodat-25M1). Crystal growth was carried out on seed plates from the Volyn Deposit (Ukraine) with size of 2÷4x6x50÷70 mm. Seed plates were cut parallel to the faces of the pinacoid {001}, then, was suspended on a copper frame in the lower zone of the autoclave. The charge consisting of a mixture of fragments of topaz with a size of 5-10 mm and bars of synthetic quartz with a size of 2x4x30÷50 mm were placed in the upper zone of the autoclave. Initial solutions were prepared on the basis of aqueous distillate and powdered fluorides of aluminum, alkali metals and ammonium, which were placed to the bottom of the autoclave. The addition of gallium and germanium were putted into the autoclave in the form of the respective oxides. The final composition of the solution was formed during the heating of the autoclave by dissolving all components. To create a contrast temperature difference, the zones were separated from each other by a perforated diaphragm with a total hole area of 10-15 %.

**Results.** Morphology and internal structure were studded under optical (MBS-10), polarization (Nikon Eclipse LV100pol) and scanning electron (Tescan Vega II XMU) microscopes. The phase composition was determined by electron probe microanalysis (Tescan Vega II XMU with energy dispersive spectrometer INCA Energy 450). Identification of the overgrown layer was performed by x-ray phase analysis (STOE Stadi MP) taking into account the data of electron probe microanalysis.

The most intensive growth of topaz was observed at temperatures of 600-650 °C in the direction [001]. The absolute values of growth rates do not exceed the first tenths of a millimeter per day. The maximum topaz overgrown layer was 4 mm on one side of the seed. The overgrown layer has a colorless, to pale bluish-green color (fig. 1a). The gallium- and germanium-containing aluminum-fluoride phase formed on the surface of the seed topaz and blocked the topaz growth in some experiments (fig. 1b). The surface of crystals, as a rule, smooth or covered with growth hills of the correct and complicated form, often with distinct concentric layers (fig. 1c). Thin striae parallel to the edge of the prism and rhombohedron face present on the faces of prisms often.

Other irrational growth surfaces have a rough regenerative relief composed of rhombohedral and prismatic pyramids with a transverse size of up to 0.5 mm. In polarized light in the overgrown layer a thin fibrous texture of the overgrown layer is often shown, caused by the regenerative growth mechanism of some faces (fig. 1d).

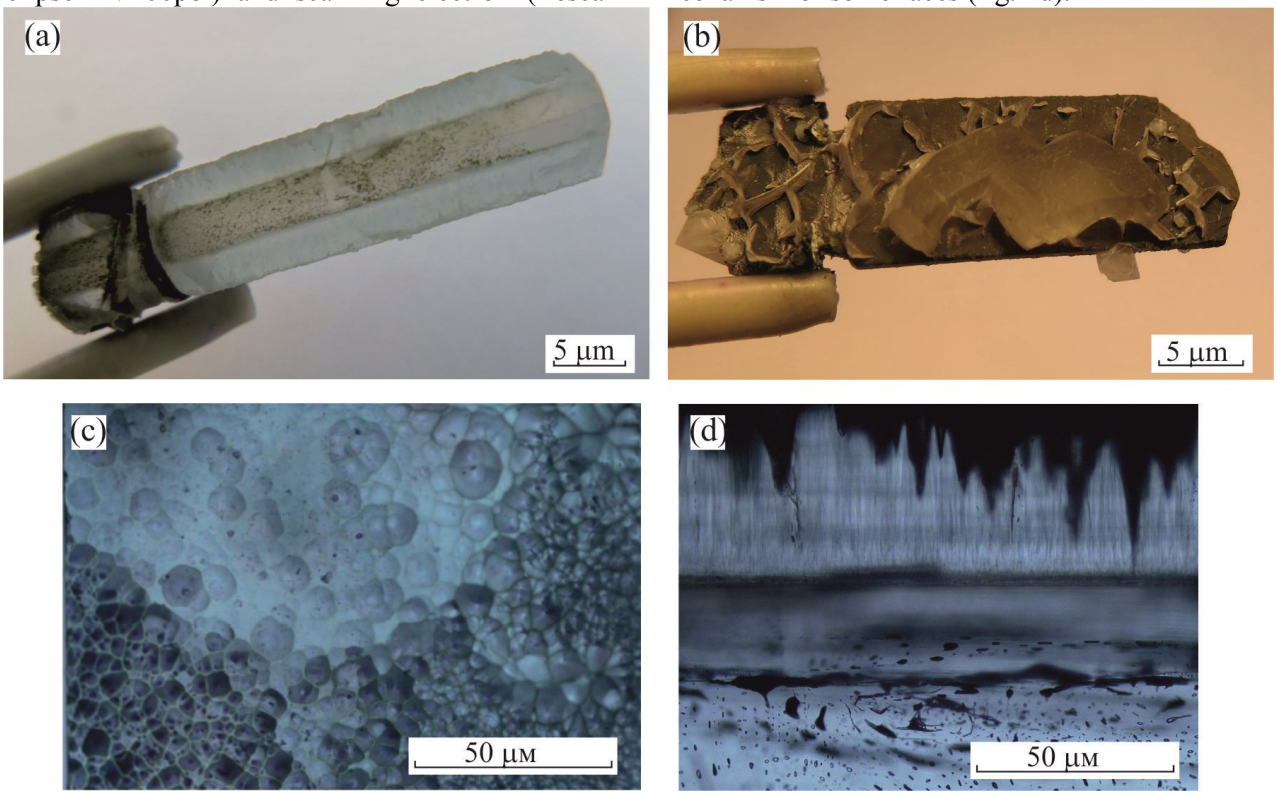


**Fig. 1.** Crystal of Ge, Ga-containing topaz (a); {001}-topaz seed with partially formed aluminium-fluoride phase Ge and Ga and an overgrown layer Ge, Ga-containing topaz (b); vicinal surface of the pinacoid face {001} (c); regenerative relief of the overgrown layer formed from rhombohedral growth pyramids (d).

**Table 1.** Composition of the overgrown layer of Ge-, Ga-containing topaz and seed of natural topaz

| Spectra | Analyzed zone | Composition | | | | | |
|---|---|---|---|---|---|---|---|
| | | $SiO_2$ | $GeO_2$ | $Al_2O_3$ | $Ga_2O_3$ | F | Total |
| 1 | Seed of natural topaz | 28.50 | 0.00 | 52.31 | 0.00 | 15.56 | 96.37 |
| 2 | | 32.44 | 0.00 | 55.89 | 0.00 | 19.95 | 108.28 |
| 3 | Overgrown layer of Ge-, Ga-containing topaz | 10.05 | 25.02 | 46.58 | 5.65 | 19.08 | 106.38 |
| 4 | | 11.15 | 23.89 | 44.07 | 5.68 | 16.87 | 101.66 |
| 5 | | 11.62 | 23.96 | 45.79 | 5.29 | 17.27 | 103.93 |
| 6 | | 21.72 | 11.82 | 51.17 | 3.36 | 18.43 | 106.50 |
| 7 | | 24.81 | 4.66 | 51.63 | 2.40 | 17.76 | 101.26 |
| 8 | | 27.04 | 3.13 | 54.54 | 2.06 | 19.00 | 105.77 |
| 9 | | 28.21 | 2.30 | 54.76 | 1.64 | 19.75 | 106.66 |
| 10 | | 29.06 | 1.15 | 55.58 | 2.34 | 19.99 | 108.12 |
| 11 | | 28.97 | 0.89 | 54.30 | 1.18 | 20.21 | 105.55 |

The EMPA showed zonal distribution of gallium and germanium in the overgrown layer (table 1, fig. 2). Zone up to 100 μm thick is formed on the border of the overgrown layer with the seed with a maximum content of germanium and gallium up to 25 wt.% $GeO_2$ and 5.7 wt.% $Ga_2O_3$ respectively (points 3-5). In the next zone up to 3 mm thick there is a sharp decrease in the content of germanium to 1 wt.% $GeO_2$ (points 6-11). The content of gallium in this zone gradually decreases from 5 to 1 wt.% $Ga_2O_3$. This is probably due to the kinetic features of dissolution of silicon, germanium, aluminum and gallium oxides.

**Conclusions.** Thus, for the first time by the hydrothermal method of temperature difference using alkaline fluoride solutions at a temperature of 600-650 °C and a pressure of 100 MPa, the topaz single crystals doped simultaneously with gallium and germanium were grown onto seed. The maximum thickness of the overgrown layer (Ga, Ge)-containing topaz parallel to the face of the pinacoid {001} is 4 mm on one side of the seed. EMPA showed the distribution of germanium and gallium in the overgrown layer is sharply uneven. The maximum content of these elements in the overgrown layer reaches 25 wt.% $GeO_2$, and 6 wt.% $Ga_2O_3$ and observed in the earliest zones of crystal growth of topaz.

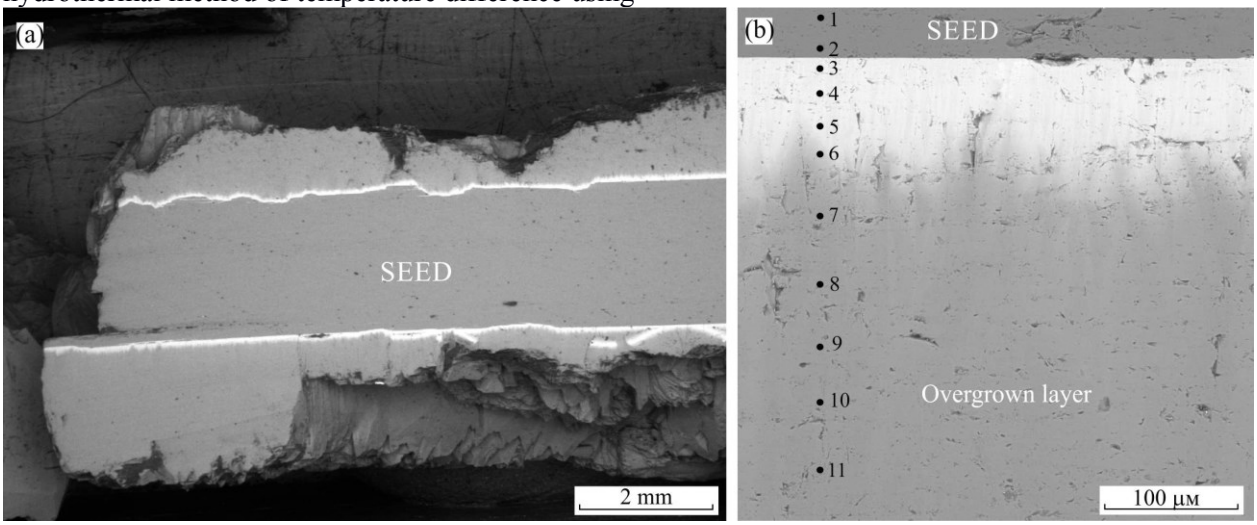


**Fig. 2.** SEM-image of an overgrown layer of Ge-, Ga-containing topaz on a natural seed (a), an enlarged image in the boundary of the seed and the overgrown layer (b), the points correspond to the spectrum numbers in table 1.

**Acknowledgments.** The reported study was funded by RFBR, project number 17-05-00976 and 18-05-00332.

**References:**

Balitsky V.S., Balitskaya L.V., Lu T., Shigley J.E. (2002) Experimental study of the simultaneous dissolution and growth of quartz and topaz. Journal of Crystal Growth. 237–239, 833–836.

Gatta G. D., Morgenroth W., Dera P., Petitgirard S., Liermann H.P. (2014) Elastic behavior and pressure-induced structure evolution of topaz up to 45 GPa. Phys. Chem. Minerals, 41, 8, 569–577.

Naumov, G.B., Ryzhenko, B.N., and Khodakovsky, I.L. (1974): Handbook of thermodynamic data. U.S. Geological Survey, Water Resources Division, 328 p

Schlüter J., Geisler T., Pohl D., Stephan T. (2010) Krieselite, $Al_2GeO_4(F,OH)_2$:A new mineral from the Tsumeb mine, Namibia, representing the Ge analogue of topaz. N. Jb. Miner. Abh. 187/1, 33–40.

Wunder B. (1997) Ge-analogues of aluminium silicates: High-pressure synthesis and properties of orthorhombic $Al_2GeO_4(OH)_2$. Eur. J. Mineral., 9, 1147-1158.

## Bublikova T.M.[1], Balitsky V.S.[1], Timokhina I.V., Setkova T.V.[1], Nekrasov A.N.[1], Krikunova P.V.[2] Morphological features of some textural varieties of natural and synthetic malachite

[1]Korzhinskii Institute of Experimental Mineralogy (IEM) RAS, Chernogolovka (tmb@iem.ac.ru), [2]Department of Geology, Lomonosov MSU, Moscow

**Abstract.** Malachite – a basic copper carbonate [$Cu_2CO_3(OH)_2$] was synthesized in crystallizer (open flow system) according to the method developed in VNIISIMS. A complex solution of ammonium hydroxide and copper sulfate was used. The growth of malachite occurred on crystallizer walls, vertically located seeds and directly on the heaters. Grown malachite specimens have a fine-patterned texture. The chemical composition and features of the internal structure of synthetic malachite were studied in comparison with natural congolese malachite with a similar patterned texture (Kolwezi deposit, DR Congo). The differences in the shape and structure of the aggregates of different origin malachites, as well as the chemical composition and the impurities content were established.

***Keywords**: malachite, synthesis, ammonium solution, copper sulphate solution, malachite aggregates, spherulites, pseudomalachite*

Malachite – a basic copper carbonate [$Cu_2CO_3(OH)_2$] is a typical mineral for the oxidation zone of copper sulphide deposits. The crystallization conditions of the malachite were studied at its synthesis with used ammonia copper sulfate solutions in a flow open system (Timokhina et al., 1983; Bublikova et al., 2019). Synthetic malachite by its physicochemical properties practically does not differ from natural malachite, but in terms of texture it is represented by only one, a banded, fine-patterned variety. The details of internal structure of obtained malachite were studied and compared with natural malachite from the Kolwezi deposit, DR Congo.

Experiments on the malachite synthesis were performed in the glass two-liter crystallizer placed in the sealed plexiglass box. The vertical heater was placed inside the crystallizer, temperature was controlled by chrome-coppel thermocouples. The synthetic malachite formed on the plates of malachite of round and square section size 5 – 10 mm, length 10 – 15 cm. An aqueous solution of copper sulfate $CuSO_4 \cdot 5H_2O$ at 0.05 – 1.0 *M* concentration was used as a working solution, then ammonium hydroxide of 20 – 25 wt % concentration was added to the solution to achieve a pH of ≈ 8 – 9. The prepared solution was delivered to the crystallizer through silicon tubes filled with silicon carbide inertial to the working solution. Solution flow rate was changed depending on the tubes diameter and on the size of powder grains. To provide constant solution mixing carbon dioxide was continuously supplied to the crystallizer. Temperature at the crystallization zone of malachite was maintained at 60 – 80 °C, periodically changing it to 5 – 10 °C every 7 – 10 days. Duration of the experiments was 25 – 35 days.

The synthesized phases, as well as natural samples were identified on the basis of X-ray powder patterns taken on a Bruker D8-advance diffractometer. Internal structure and chemical composition of the samples were studied on the fractures and polished surfaces using a Tescan Vega II XMU scanning electron microscope with an INCA Energy 450 energy dispersive spectrometer (EDS).

Chemical compositions of the studied samples of synthetic and natural malachite presented in Table 1. Insignificant content of $SO_3$ presents in the synthesized malachite samples due to the technological additives according to the method (Bublikova et al., 2000), however Si and Ni present due to the use in the process of synthesis chemical reagents containing these elements. The major difference in the chemical composition of congolese malachite and synthetic malachite is about high phosphorus content (to 5 – 6 wt % $P_2O_5$) in the most natural samples. In the samples with phosphorus content from 5 to 25 wt % $P_2O_5$ a inclusions of pseudomalachite $Cu_6(PO_4)_2(OH)$ are present as round bright spots with diameter to 1 – 2 mm.

**Table 1.** Chemical composition of synthetic malachite and natural malachite samples, wt %

| Component | $K_2O$ | NiO | CuO | $SiO_2$ | $P_2O_5$ | $SO_3$ |
|---|---|---|---|---|---|---|
| Synthetic malachite (VNIISIMS) | – | 0.25–0.50 | 62.77–65.26 | 0.25–0.28 | – | 0.15–0.41 |
| Natural malachite (DR Congo) | 0–0.21 | – | 67.03–69.35 | 0.12–0.35 | 0.21–5.85<br>5.92–23.48* | – |

*The samples of natural malachite contain pseudomalachite impurities $Cu_6(PO_4)_2(OH)$;
– a line means that the content is below the detection limit by the X-ray spectral microanalysis

The synthetic malachite obtained in our experiments has the thickness of the accretion layer within 15 – 18 mm. Malachite grown on vertical seeds and also on the sides of crystallizer has a fine-patterned texture with contrast zonality alternation of different shades of green (Fig. 1a). In every zone we observe the phenomenon of geometrical selection among spherulites. Visually distinguishable layers of light-green color are built by small malachite aggregates (20 – 30 μm) and dark-green up to black layers are formed by larger aggregates (300 – 400 μm). Relatively small spherulites built up by crystals up to 20 μm with thickness 1 – 2 μm gradually replaced by larger spherulites. Crystals have a long-prismatic habit and are often flattened (Fig. 1b). Groups of spherulites form malachite buds diameter to 1 – 5 mm. Research of the internal structure of malachite obtained from different experiments showed the presence of pores and small irregular-shaped cavities between spherulites as well as malachite buds. During the crystallization process of malachite from concentrated ammonium copper solution, a continuous mass origination of small malachite particles occurs on the whole seed surface and crystallizer walls. These particles become centers of growing spherulites, which unequally grow in different directions until they contact with neighboring spherulites. Free space remains between the surfaces of contacting spherulites and buds. Fresh solution recharge doesn't happen if the cavity is isolated and tightly closed by neighboring aggregates. More often loose and small-grained malachite crystallizes from remaining solution on the cavity walls. The solution may evaporate after ending of the experiment if the cavity is leaky. In rare cases in fine-patterned malachite grown on horizontal surface (bottom part of the seed) were observed thin layer thick several μm of parallel located aggregates, which made of prism habit crystals thick 1 – 2 μm which then replaced by a new layer of spherulites (Fig. 1c).

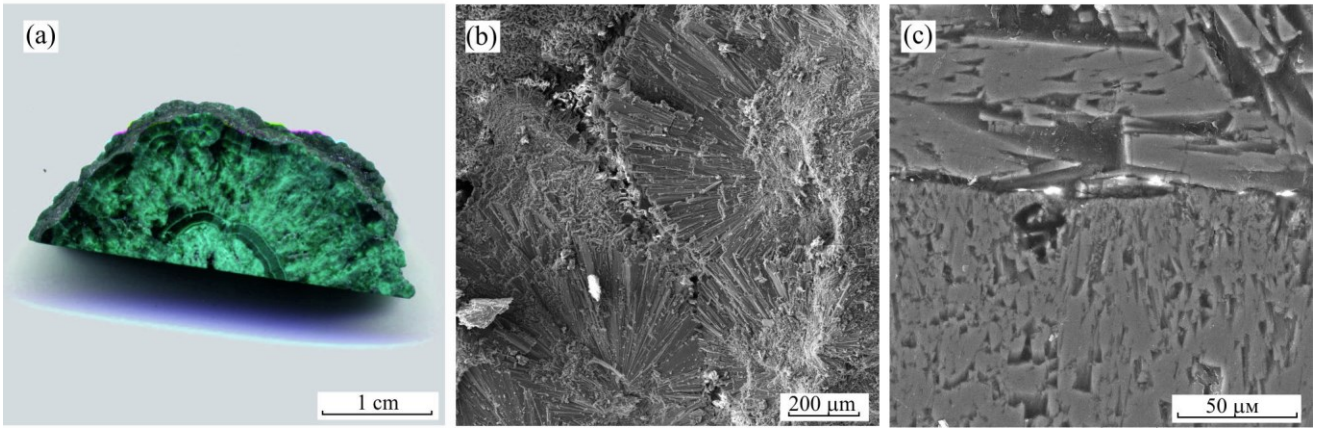


**Fig. 1** (a) – sample of synthetic malachite with fine- patterned texture grown in the opened flowing system (All-Russia Research Institute of Raw Mineral); (b) – spherulites composing a malachite buds; (c) – prismatic malachite crystals (growth on the horizontal part of the seed); (b, c) – secondary electron images.

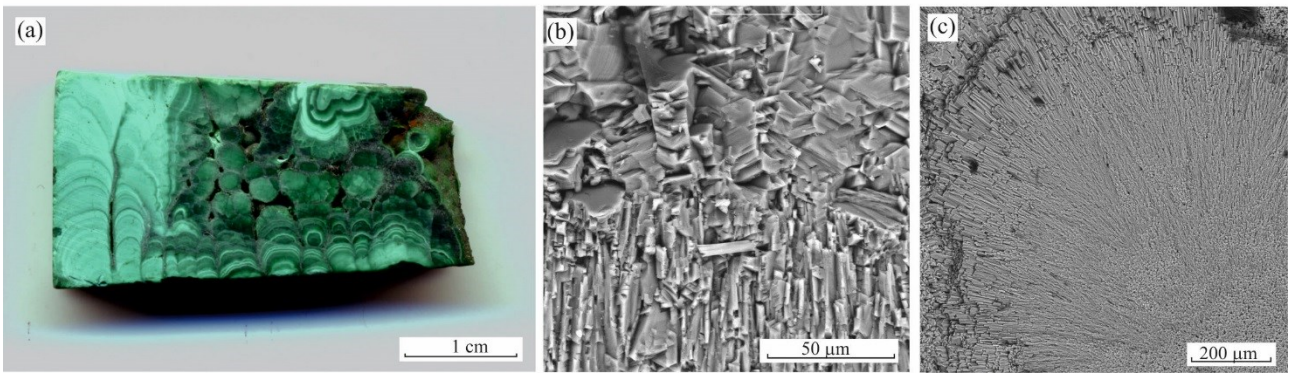


**Fig. 2** (a) – sample of natural malachite with combined patterned texture (Kolwezi deposit, DR Congo); (b) – parallel-columnar aggregates and (c) – spherulites composing natural malachite.

The major part of malachite exported to Russia mined on DR Congo deposits is presented by parallel-banded and wavy-banded malachite, less often occur malachite with concentric-zonal, patterned, laced, breccia textures (Mukendy, 2009; Chernenko, Melnikov, 2003). To study and compare features of the internal structure of natural and synthetic malachite we selected samples of malachite with combined patterned texture, which is a combination of fine wavy-banded and fine-patterned textural varieties (Fig. 2a). Internal structure of two zones (wavy-banded and fine-patterned) of the sample significantly differ. Alternate layers of light-green and green color of banded malachite are

formed by parallel-columnar aggregates (Fig. 2b). Aggregates consist of ordered parallel located elongated prismatic crystals thick 2 – 5 μm and located perpendicular to growing layer of malachite (Fig. 2b, the lower part of the picture). Layer color is light-green. Next layer with more intensive dark color consists of bigger aggregates angled to previous layer, a crystal sizes vary from 10 to 20 μm. Visually wavy different-colored layers create an effect of lace. The central part of a sample is formed by blocks of big visually distinguishable spherulites diameter 0.5 – 1.5 mm. Radially located crystals making spherulites have a prismatic habit, they are elongated with thick 3 – 10 μm (Fig. 2c). Various combinations of zones having different structure with the alteration of different-colored layers and impregnations of pseudomalachite with bright dark-green color in one sample of malachite form the unique non-repeating pattern of natural malachite.

In this way, principal differences in the structure of synthetic and natural malachite of close textural varieties are in form, sizes and structure of forming them mineral aggregates. Synthetic fine-patterned malachite obtained in the open flowing system (VNIISIMS) in most cases has a bud-like structure. Spherulites forming the bud consists of crystals of long prismatic habit often flattened. In studied samples of the patterned natural congolese malachite, the variety of textural pattern is made by alteration and various combinations of zones, which consist of parallel-column aggregates with areas formed by spherulites. Additional contribution to the textural pattern of congolese malachite make impregnations of pseudomalachite.

**References:**


Bublikova T. M., Balitsky V. S., Khanin D. A., Nekrasov A. N., Setkova T. V. // Features of the Internal Structure of a Synthetic Malachite. Moscow University Geology Bulletin // 2019. Vol. 74. No. 1. P. 73–80.

Bublikova, T.M., Balitsky, V.S., and Timokhina, I.V. Synthesis and Main Properties of Jeweler–Ornamental Malachite. Synthesis of Minerals. Aleksandrov, VNIISIMS, 2000. Vol. 1. 662 p.

Chernenko, T.V. and Mel'nikov, E.P. Properties and diagnostics of natural and synthetic malachite // Vestn. Gemmol. 2003. № 8. P. 11–26; № 9. P. 31–35.

Mukendi E.B. Criteria of the geological–commercial assessment of malachite from the Democratic Republic of the Congo. Cand. Sci. (Geol.-Min.) Dissertation. Moscow: Mosk. Geol.-Razved. Inst. 2009. 26 p.

Timokhina I.V., Balitsky V.S., Shaposhnikov A.A., Bublikova T.M., Akhmetova G.L., Dubovskii A.A. Physicochemical studies of synthetic malachite // Dokl. Akad. Nauk SSSR. 1983. Vol. 270. P. 1117–1119.



**Kotelnikov A.R.[1], Akhmedzhanova G.M.[1], Suk N.I.[1], Schipalkina N.V.[2], Kotelnikova Z.A.[3], Kovalskaya T.N.[1], Van K.V.[1]**


**Experimental study of gallium feldspars** UDC 550.4:549.651.1


[1]Institute of Experimental Mineralogy RAS (IEM RAS), Chernogolovka Moscow district, (kotelnik@iem.ac.ru; sukni@iem.ac.ru); [2]M.V. Lomonosov Moscow State University, Geological Faculty, Moscow; [3]Institute of Geology of Ore Deposits, Petrography, Mineralogy, and Geochemistry RAS (IGEM RAS), Moscow (kotelnik@igem.ac.ru)



**Abstract.** The cation-exchange equilibria in the gallium feldspar – fluid system were studied: $NaGaSi_3O_8$ss + KClaq = $KGaSi_3O_8$ss + NaClaq. The experiments were carried out according to the ampoule technique at T=550°C and P=1.5 kbar. Based on the data on the of sodium and potassium distribution between feldspars and fluid, as well as the boundaries of the solid solution decomposition region, excess mixing energies were calculated. The parameters of the elementary cells of synthetic gallium alkali feldspar were refined. It is shown that sodium feldspars belong to the structural type C1, and potassium differences – to C2/m. The concentration dependences of the parameters of the elementary cells are given. Excess mixing volumes of feldspar solid solution were calculated. A comparison of the functions of mixing gallium feldspar with other solid solutions of frame aluminosilicates is carried out.



***Keywords:*** *experiment, feldspar,* parameters of elementary cells, solid solution, excess mixing volumes


**Introduction** Gallium alkaline feldspars of the $NaGaSi_3O_8$ – $KGaSi_3O_8$ series are interesting for studying the properties of minerals of the frame aluminosilicate group, as well as models of solid solutions in which structural ordering largely determines their thermodynamic properties. Under natural conditions, gallium feldspars $(Na_xCa_{1-x})Ga_{2-x}Si_{2+x}O_8$ are found in fluid inclusions in sphalerite from Almadena deposit (Spain). It is known that sphalerite is a concentrator of such rare elements as gallium and indium. For the first time, Ga-feldspars were studied in the foundational work (Pentinghaus, 1980). On the basis of x-ray studies of synthetic gallium feldspars, a schematic TX diagram of solid solutions $(Na,K)GaSi_3O_8$ feldspars was constructed and an extensive area of their immiscibility was shown. The aim of our study was to study the cation-exchange equilibria of gallium feldspars with a solution: $NaGaSi_3O_8$ ss + KCl aq = $KGaSi_3O_8$ ss + NaCl aq to obtain data on excess mixing energies. It was also supposed to refine the parameters of the elementary cells of solid solutions of gallium feldspar.

**Experimental Conditions** *Starting materials.* Glasses of $NaGaSi_3O_8$ and $KGaSi_3O_8$were used as starting materials. The glasses were obtained by melting at 1200°C and a pressure of 2 kbar for 6 hours of mixtures of oxides and carbonates

preliminarily decarbonated at 1000°C. The following reagents were used to prepare these mixtures: $Na_2CO_3$, $K_2CO_3$, $Ga_2O_3$, $SiO_2$. Microprobe analysis showed the homogeneity of these glasses and their consistency with stoichiometric formulas. 1M NaCl and 1M KCl were used as solutions.

*Equipment.* All experiments were performed on high-pressure hydrothermal plants with external heating and cold-seal construction of the IEM RAS. The accuracy of the adjustment and temperature control was ± 3°C; pressure ± 50 bar. The time to enter the mode was about 1.5-2 hours. The cooling (quenching) time at the end of the experiment was 5–10 min. The duration of the experiments at 550°C and a pressure of 1.5 kbar ranged from 12 to 22 days.

*Experimental methods.* All cation-exchange experiments were performed by ampoule method. Mainly gold ampoules with a diameter of 5 mm, wall thickness 0.2 mm were used. A sample of $NaGaSi_3O_8$ and $KGaSi_3O_8$ compositions was loaded into ampoules and a solution of the required composition was poured. The ampoule was welded and weighed. The tightness test was carried out by the gravimetric method. The compositions of the initial samples were selected so that the approach to equilibrium was carried out from two sides.

*Methods of analysis.* The compositions of the experiments were determined on a Tescan Vega II XMU scanning electron microscope (Tescan, Czech Republic) equipped with an INCA Energy 450 X-ray microanalysis system with energy dispersive (INCAx-sight) and crystal diffraction (INCA wave 700) X-ray spectrometers (Oxford Instruments, England) and the INCA Energy+ software platform. The composition of the solutions was studied by the AAS method. An x-ray study of the synthesized samples was performed and the unit cell parameters were refined.

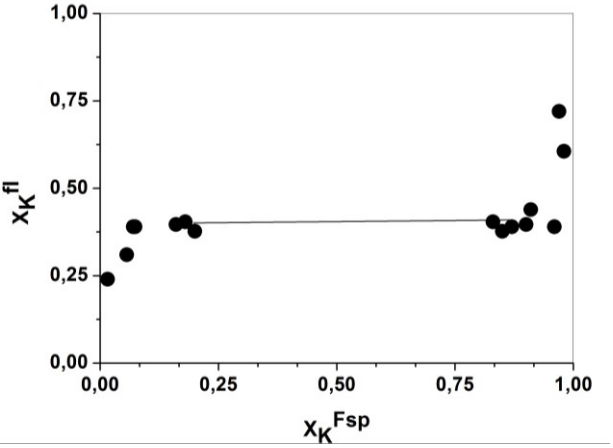


**Fig.1.** Potassium distribution between gallium feldspar and fluid at 550°C and 1.5 kbar

**Experimental results** The conditions and results of the experiments are presented in Table 1 and Figure 1. It can be seen from Figure 1 that the distribution of potassium between feldspar and fluid is not ideal. At parameters of the experiments the region of the decomposition of the solid solution was observed. The boundaries of the decay region (n=5) are as follows: $X_K^{(1)}$ = 0.14(6); $X_K^{(2)}$ = 0.88(5). The calculation of the parameters of the solid solution according to Margules along the boundaries of the decay region (Kotelnikov, 1995) yielded the following parameter values: W1 = 17.83 (± 0.18) and W2 = 18.37 (± 0.15) kJ/mol (at 550°C).

**Table 1**. Conditions and results of experiments on the cation exchange of solid solutions (Na,K)$GaSi_3O_8$ with fluid (550 ° C and 1.5 kbar)

| № exp. | Hitch* | $X_K^{fl}$, д/о | Duration, days | $X_K^{Nafsp}$ п/о | $X_K^{Kfsp}$ п/о | n | $X_K^{fl}$, п/о |
|---|---|---|---|---|---|---|---|
| 7229 | 100 mg Ga-Ab gl. | 1 | 12 | 0.074(9) | 0.87(2) | 17 | 0.39 |
| 7230 | 100 mg Ga-Ksp gl. | 0 | 12 | 0.16(1) | 0.90(4) | 12 | 0.396 |
| 7231 | 100 mg Ga-Ab gl. | 0.5 | 12 | 0.07(2) | 0.96 | 10 | 0.39 |
| 7232 | 100 mg Ga-Ksp gl. | 0.5 | 12 | - | 0.98(2) | 5 | 0.606 |
| 7233 | 50 mg Ga-Ab gl. + 50 mg Ga-Ksp gl. | 0 | 12 | 0.18(5) | 0.83(5) | 5 | 0.404 |
| 7234 | 50 mg Ga-Ab gl. + 50 mg Ga-Ksp gl. | 1 | 12 | 0.20(7) | 0.85(5) | 11 | 0.377 |
| 7247 | 150 mg Ga-Ksp gl. | 0.72 | 20 | - | 0.97(3) | 10 | 0.72 |
| 7248 | 150 mg Ga-Ab gl. | 0.20 | 20 | 0.016(5) | - | 6 | 0.24 |
| 7253 | 100 mg Ga-Ab gl. | 0.30 | 25 | 0.056* | - | - | 0.31 |
| 7254 | 100 mg Ga-Ksp gl. | 0.40 | 25 | - | 0.91* | - | 0.439 |

* bulk analysis; n is the number of analyzes.

**Table 2.** Parameters of unit cells of (Na,K) $GaSi_3O_8$

| № exp | $X_K^{Fsp}$ | a,[A] | b, [A] | c, [A] | α, [°] | β, [°] | γ, [°] | V, $[A]^3$ |
|---|---|---|---|---|---|---|---|---|
| PDF | 0 | 8.166 | 12.858 | 7.204 | 94.37 | 116.52 | 87.14 | 674.6 |
| 7248 | 0.020 | 8.163(1) | 12.869(2) | 7.207(1) | 94.37(2) | 116.52(1) | 87.14(2) | 675.9(2) |
| 7229 | 0.074 | 8.202(1) | 12.877(1) | 7.202(1) | 93.85(1) | 116.44(1) | 87.46(1) | 679.5(2) |
| 7231 | 0.070 | 8.201(1) | 12.878(1) | 7.201(1) | 93.84(1) | 116.45(1) | 87.47(1) | 679.3(2) |
| 7233 | 0.092 | 8.205(1) | 12.877(1) | 7.200(1) | 93.80(1) | 116.39(1) | 87.49(1) | 679.9(2) |
| 7234 | 0.150 | 8.252(1) | 12.932(1) | 7.218(1) | 93.53(1) | 116.28(1) | 87.88(1) | 689.4(2) |
| 7230 | 0.160 | 8.243(1) | 12.918(1) | 7.210(1) | 93.34(1) | 116.38(1) | 87.81(1) | 686.1(2) |
| 7233 | 0.800 | 8.560(3) | 13.110(2) | 7.229(1) | 90.0 | 116.11(1) | 90.0 | 728.5(4) |
| 7229 | 0.870 | 8.610(2) | 13.093(2) | 7.218(1) | 90.0 | 116.10(1) | 90.0 | 730.8(3) |
| 7230 | 0.900 | 8.612(1) | 13.100(1) | 7.235(1) | 90.0 | 116.11(1) | 90.0 | 733.5(2) |
| 7231 | 0.960 | 8.642(4) | 13.107(5) | 7.235(3) | 90.0 | 116.11(1) | 90.0 | 735.8(7) |
| 7232 | 0.980 | 8.653(1) | 13.108(1) | 7.240(1) | 90.0 | 116.07(1) | 90.0 | 737.7(1) |
| 7247 | 0.980 | 8.667(1) | 13.083(1) | 7.225(1) | 90.0 | 116.12(1) | 90.0 | 735.4(1) |
| PDF | 1.00 | 8.661 | 13.110 | 7.239 | 90.0 | 116.08 | 90.0 | 738.8 |

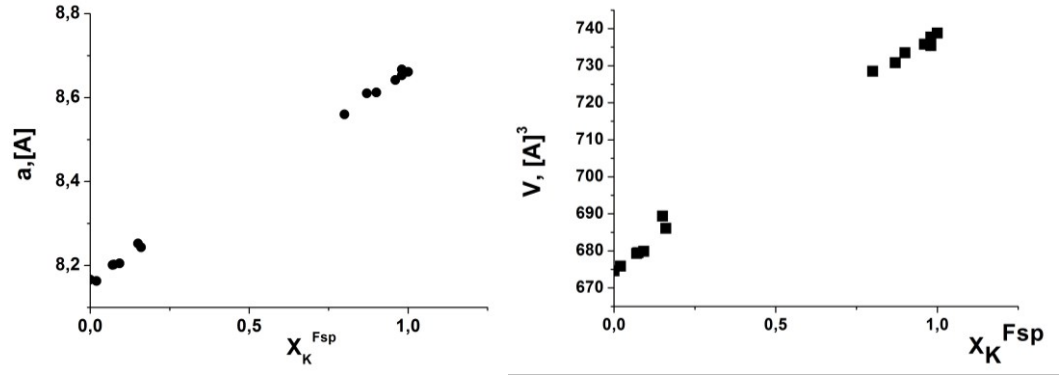


**Fig. 2.** Concentration dependences of unit cells parameters of solid solutions (Na,K) $GaSi_3O_8$.

**X-ray study of solid solutions of gallium feldspar** The refined values of the parameters of the elementary cells are given in Table 2. Figure 2 shows the concentration dependences of elementary cells parameters. Based on the dependence of $(\cos^2\alpha)*1000$ on the composition of the solid solution, the point of the C1 → C2/m structural transition was determined: this transition occurs at $X_K^{Fsp}$ = 0.39±0.02. Apparently, the immiscibility region is associated precisely with this structural transition.

**Conclusions**

1. Based on cation-exchange experiments, an isotherm of potassium distribution between the solid solution (Na,K)$GaSi_3O_8$ and the equilibrium fluid was constructed. The immiscibility region of the solid solution was found.
2. Along the boundaries of the solid solution immiscibility region, the parameters of the Margules model were calculated.
3. The parameters of the elementary cells of the solid solution of gallium feldspar and their concentration dependences are specified.
4. Based on the dependence of (cos2α)*1000 on the composition of the solid solution, the point of the structural transition C1 → C2/m is determined.

**References:**

1. Kotelnikov A.R. Isomorphism in frame aluminosilicates. Author's abstract Dr. dissert. Moscow. 1995. 41 p.
2. Pentinghaus H. Polymorphie in den feldspatbildenden systemen A+T3+T4+O8 und A2+T23+T24+O8 alkali- und erdalkali-, bor-, aluminium-, gallium-, eisen-silikate und -germanate. Habil.Diss. 1980. Munster. 210 s.

## Kotelnikov A.R.[1], Schipalkina N.V.[2], Suk N.I.[1] Synthesis of as-containing feldspars and feldspathoids UDC 550.89

[1]Institute of Experimental Mineralogy RAS (IEM RAS), Chernogolovka Moscow district, (kotelnik@iem.ac.ru; sukni@iem.ac.ru); [2]M.V. Lomonosov Moscow State University, Geological Faculty, Moscow

**Abstract.** Feldspars with an isomorphic $2Si^{4+} \leftrightarrow Al^{3+} + As^{5+}$ substitution, synthetic analogs of the filatovite $KAl_2SiAsO_8$, were synthesized. The starting materials were glass of filatovite composition, obtained by fusing of potassium meta arsenate ($KAsO_3$) and sillimanite gel ($Al_2SiO_5$) at 1300°C for 6 hours. The experiments were carried out at T=600-650°C, a P=1-1.5 kbar in gold

ampoules. To maintain the required oxygen potential, a 10% $H_2O_2$ solution was added to the ampoules. Experiments were carried out in hydrothermal apparatus with external heating and cold seal. The products of the experiments were studied by X-ray and microprobe methods. In the products of the experiments, a mixture of phases consisting of crystals of filatovite, As-containing kalsilite, and wrightite ($K_2Al_2O[AsO_4]_2$) was fixed. Phase compositions and X-ray data are given.

***Keywords:*** *experiment, feldspar,* feldspathoids, synthesis*, unit cells parameters*

Filatovite with averaged formula $KAl_2SiAsO_8$ is arsenic feldspar from fumarole vlc. Tolbachik was first studied and described in work of Vergasova et al. (2004) (Fig. 1). Previously, phosphorus-containing potassium feldspar was synthesized with the crystal-chemical formula $KAl_2SiPO_8$ (Simpson, 1977; Bychkov et al., 1989). In these feldspars, an isomorphic substitution of the type $2Si^{4+} \leftrightarrow Al^{3+}+P^{5+}(As^{5+})$ takes place. We decided to carry out the synthesis of filatovite in the laboratory.

**Experimental methods**

*Starting materials.* For the synthesis of filatovite, it was decided to use $KAl_2SiAsO_8$ glass, since other starting substances, for example, gel mixtures, were inapplicable due to differences in the solubility of their components. Ortho-arsenic acid salts (orthoarsenates) are actively hydrated even with moisture from the air, so it was difficult to use them. Potassium meta arsenate – $KAsO_3$ is much more convenient. Potassium meta arsenate was prepared as follows. First, by oxidation of metallic arsenic in hydrogen peroxide (30 wt.%) orthoarsenate acid was obtained: $2As_{met} + H_2O_2 + 2H_2O = 2H_3AsO_4$. This reaction proceeds with a large heat release. To prevent boiling up, the reaction vessel must be cooled. Then, adding the required amount of potassium hydroxide to the solution, and evaporating the solution, we obtained potassium metaarsenate: $H_3AsO_4 + KOH = KAsO_3 + 2H_2O\uparrow$. The evaporation process is well carried out in glassy carbon cups. Potassium metaarsenate practically does not absorb moisture and it is convenient to work with it. We mixed potassium metaarsenate and a sillimanite gel under a layer of alcohol in a jasper mortar: $KAsO_3 + Al_2SiO_5 = KAl_2SiAsO_8$. The resulting mixture was dried for 2-3 hours at 150°C in a drying oven. After that, the mixture was poured into a platinum crucible and kept at 1300°C in a KO-14 laboratory furnace. Warming up to a predetermined temperature was carried out for 6 hours. Exposure at 1300°C was 2 hours. Microprobe analysis showed the homogeneity of the glass in composition. Occasionally, needle crystals of corundum with a size of 20x2-3 microns were found in glass.

*Equipment.* All experiments were carried out on hydrothermal installations with external heating and cold gate of the IEM RAS construction. The accuracy of temperature maintenance was ±5°C and pressure ±50 bar. Pyrosynthesis experiments were performed in a KO-14 furnace. The accuracy of the temperature adjustment was also ±5°C.

*Experimental methods.* Experiments on the synthesis of filatovite were carried out in gold ampoules, which were loaded with 75-100 mg of $KAl_2SiAsO_8$ glass and poured with 5 μl of 10% hydrogen peroxide solution. Hydrogen peroxide is needed to maintain the required oxygen potential. Ampoules were brewed and placed in reactors. The duration of the experiments at 650°C and 1.5 kbar was 14 days. The tightness control was carried out by the gravimetric method. Also experiments on dry crystallization of glass (pyrosynthesis) at 750°C and atmospheric pressure were carried out in a muffle furnace. The duration of pyrosynthesis was 30 days.

*Methods of analysis*. The products of the experiments were analyzed on a Tescan Vega II XMU scanning electron microscope (Tescan, Czech Republic) equipped with an INCA Energy 450 X-ray microanalysis system with energy dispersive (INCAx-sight) and crystal diffraction (INCA wave 700) X-ray spectrometers (Oxford Instruments, England) software platform INCA Energy+, and also studied by x-ray method. The parameters of the elementary cells of the synthesized phases were refined.

**Experimental results**

Feldspars with isomorphic substitution of $2Si^{4+} \leftrightarrow Al^{3+} + As^{5+}$, synthetic analogs of the filatovite $KAl_2SiAsO_8$ were synthesized. In the products of the experiments, a mixture of phases, consisting of crystals of filatovite, As-containing kalsilite, and wrightite ($K_2Al_2O[AsO_4]_2$) was recorded (Fig. 2). Under hydrothermal conditions, arsenic-containing feldspars, kalsilites containing As, and a certain amount of mineral wrightite are synthesized. Their compositions are given in table.1.

In addition to kalsilite and filatovite, individual grains of mineral wrightite were found in the products of the experiments. Recalculating its composition into 9 atoms (O) gave the following formula $K_{1.819}Al_{1.554}Si_{0.337}O_{0.864}[AsO_4]_{2.034}$. As can be seen from table 1, the compositions of synthetic As-feldspars vary slightly, which indirectly indicates their equilibrium synthesis. In the same time arsenic containing kalsilit are characterized by significant compositional variations (Table 1). It is shown that isomorphic substitutions of the type $2Si^{4+} \leftrightarrow Al^{3+} + As^{5+}$ are carried out in kalsilites. The dependence 2Si = f(Al+As) has a high correlation coefficient ($r_{xy}$ = 0.996) and is described by the regression equation: Si = 4.257-2.224 * (Al+As); r = 0.996; Sx = 0.014; Ex = 0.012.

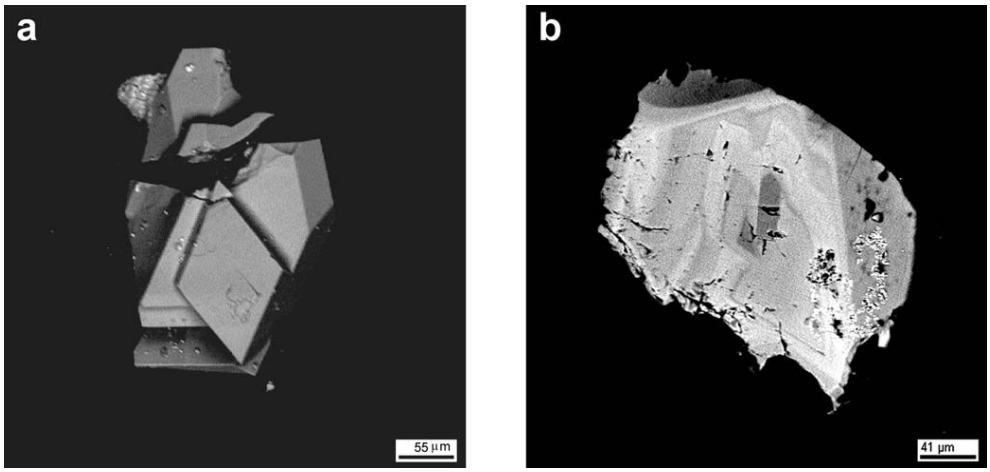


**Fig. 1.** Filatovite crystals $K[(Al,Zn)_2(As,Si)_2O_8]$ from vlc. Big Tolbachik, fumarole formations (Vergasova et al, 2004).

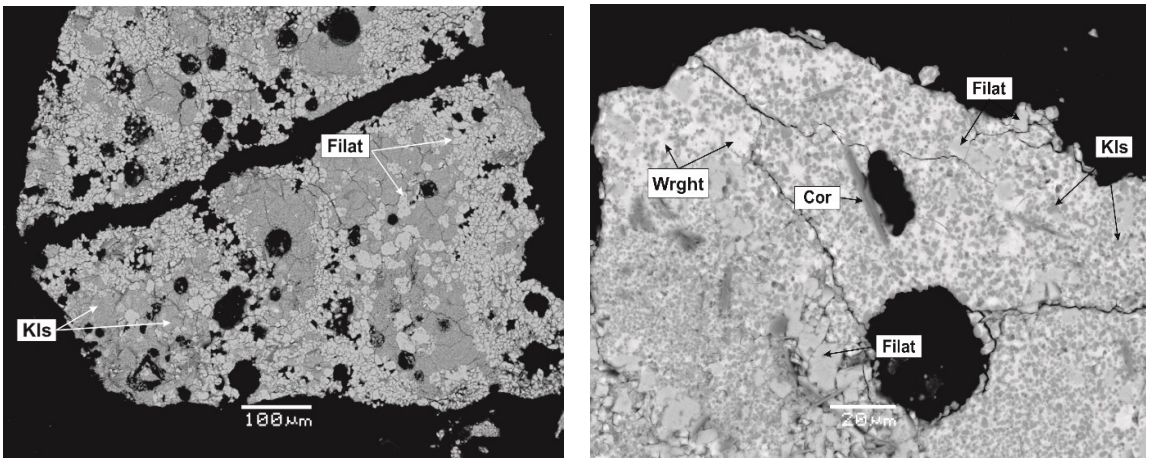


**Fig. 2** Products of experiments on hydrothermal synthesis of filatovite. Kalsilit (Kls), filatovite (Filat) and wrightite (Wrght) crystals are visible.

**Table 1.** The compositions of synthetic filatovite and kalsilit (wt.%).

| Filatovite | | | | Kalsilit | | | |
|---|---|---|---|---|---|---|---|
| Oxide | Average | Variation | Ex | Oxide | Average | Variation | Ex |
| $K_2O$ | 12.48 | 12.05 ÷ 13.31 | 0.57 | $K_2O$ | 27.04 | 24.33 ÷ 29.23 | 1.81 |
| $Al_2O_3$ | 32.13 | 31.17 ÷ 32.47 | 0.59 | $Al_2O_3$ | 32.35 | 30.95 ÷ 34.00 | 1.03 |
| $SiO_2$ | 19.92 | 19.58 ÷ 20.35 | 0.35 | $SiO_2$ | 33.25 | 28.70 ÷ 37.62 | 3.08 |
| $As_2O_5$ | 35.52 | 34.52 ÷ 36.75 | 0.93 | $As_2O_5$ | 5.70 | 0.10 ÷ 13.54 | 4.57 |
| Sum | 100.05 | - | - | Sum | 98.34 | - | - |
| Formula (recalculated to 8 O atoms): $K_{0.844}Al_{2.009}Si_{1.054}As_{0.982}O_8$ | | | | Formula (recalculated to 4 O atoms): $K_{0.930}Al_{1.027.896}As_{0.081}O_4$ | | | |

**Table 2**. Parameters of unit cells of synthetic phases.

| Sample | Space group | a, [A] | b, [A] | c, [A] | β, [°] | V, $[A]^3$ | Ref.* |
|---|---|---|---|---|---|---|---|
| Filatovite synthetic | I2/c | 8.738(4) | 13.330(5) | 14.767(5) | 115.96(3) | 1536(1) | 1 |
| Filatovite nature | I2/c | 8.772(1) | 13.370(2) | 14.690(2) | 115.944(6) | 1549.24 | 2 |
| Kls synthetic | $P6_3$ | 5.1664(9) | 5.1664(9) | 8.717(2) | - | 201.49(7) | 3 |
| Kls – PDF | $P6_3$ | 5.161(4) | 5.161(4) | 8.693(5) | - | 200.52 | 3 |

*:
1– our data;
2 – Vergasova et al., 2004;
3 – PDF data base #85-1413

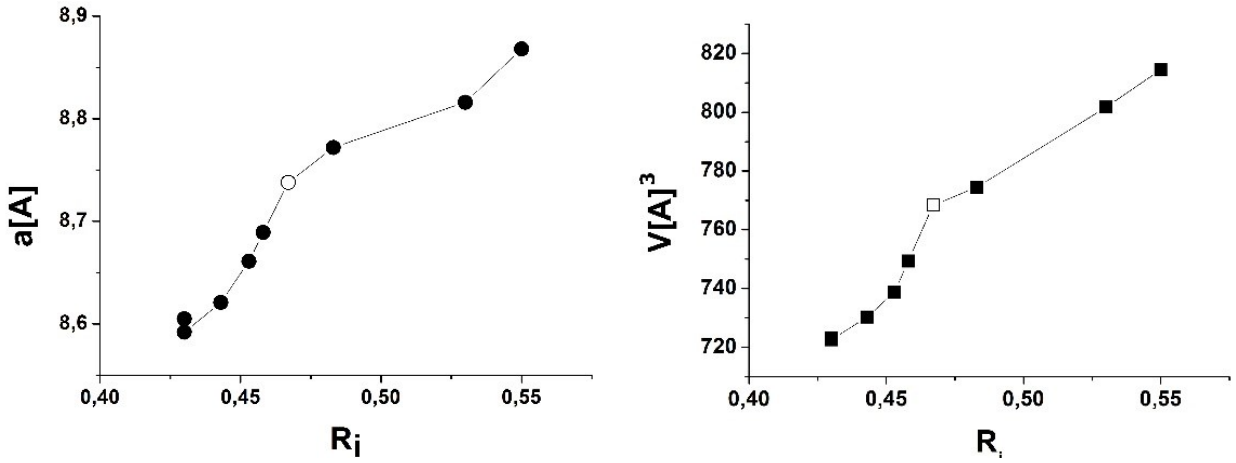


**Fig. 3.** Dependencies of the parameter (a) and the volume of the unit cell (V) of potassium feldspar (sp. gr. c2/m) on the average value of the framework-forming cation ($R_i$).

**Table 3.** Parameters of feldspar unit cells depending on the average radius of the tetrahedral cation.

| Feldspar, formula | $R_i$ [A],* average | a, [A] | b, [A] | c, [A] | α, [°] | β, [°] | γ, [°] | V,[A]$^3$ | Ref. |
|---|---|---|---|---|---|---|---|---|---|
| $KAlSi_3O_8$ -h | 0.43 | 8.605 | 13.031 | 7.177 | 90.0 | 116.00 | 90.0 | 723.3 | 1 |
| $KAl_2SiPO_8$ | 0.443 | 8.621 | 13.084 | 7.203 | 90.0 | 115.99 | 90.0 | 730.3 | 2 |
| $KGaSi_3O_8$ | 0.453 | 8.661 | 13.110 | 7.239 | 90.0 | 116.08 | 90.0 | 738.8 | 3 |
| $KFeSi_3O_8$ | 0.458 | 8.689 | 13.12 | 7.319 | 90.0 | 116.10 | 90.0 | 749.3 | 3 |
| $KAl_2SiAsO_8$ | 0.483 | 8.772 | 13.37 | 7.345 | 90.0 | 115.94 | 90.0 | 774.5 | 4 |
| $K_{0.84}Al_{2.01}Si_{1.05}As_{0.98}O_8$ | 0.467 | 8.738 | 13.330 | 7.383 | 90.0 | 115.96 | 90.0 | 768.4 | 5 |
| $KAlGe_3O_8$ | 0.53 | 8.816 | 13.55 | 7.457 | 90.0 | 115.89 | 90.0 | 801.7 | 6 |
| $KGaGe_3O_8$ | 0.55 | 8.872 | 13.631 | 7.491 | 90.0 | 115.99 | 90.0 | 814.3 | 7 |
| $KFeGe_3O_8$ | 0.56 | 8.891 | 13.703 | 7.542 | 90.0 | 115.86 | 90.0 | 826.9 | 7 |

*- $R_i=[\Sigma(X_i*R_i)]/4$; $X_i$ – mole fraction of i-cation; $R_i$ – crystal radius of i-cation.
1 - Kroll&Ribbe, 1987; 2 - Simpson, 1977; 3 - Pentinghaus, 1980; 4 - Vergasova, e.a. 2004; 5 – our data;
6 - Kroll, et.al, 1991; 7 - Pentinghaus, 1970.

The parameters of the unit cells of the synthesized phases are refined. The data are shown in table 2.

Table 3 and figure 3 show the dependence of unit cells parameters on the average size of the framework-forming tetrahedron (Al, Ga, Fe, Si, Ge, P, As) $O_4^-$.

**Conclusions**

1. In hydrothermal conditions, arsenic-containing feldspars and kalsilits were synthesized.

2. The parameters of the unit cells of the synthesized phases were refined.

3. The dependence of unit cells parameters on the average size of the framework-forming tetrahedron (Al, Ga, Fe, Si, Ge, P, As) $O_4^-$ is shown.

**References:**

Bychkov A.M., Kotelnikov A.R., Romanenko I.M., Senderov E.E. The influence of isomorphic substitution of silicon with phosphorus on the structural features of feldspars.. Geochemistry. 1989. № 2. P. 310-313.

Kroll H., Ribbe P.H. Determining (Al,Si) distribution and strain in alkali feldspars using lattice parameters and diffraction-peak positions: A review. Amer.Miner., 1987, V. 72. P. 491-506.

Kroll H., Flogel J., Breit U., Pentinghaus H.Order and anti-order in Ge- substituted alkali feldspars. Eur.J.Mineral., 1991. V. 3. P. 739-749.

Pentinghaus H. Der Einbau von Al(III), Ga(III), Fe(III) und Si(IV), Ge(IV) in syntetische Alkalifeldspate. Dissertation. 1970. Munster. 203 s.

Pentinghaus H. Polymorphie in den feldspatbildenden systemen A+T3+T4+O8 und A2+T23+T24+O8 alkali und erdalkali -, bor-, aluminium-, gallium-, eisen-silikate und germanate. Habil.Diss., 1980. Munster. 210 s.

Simpson D.R. Aluminium phosphate variants of feldspar. American Mineralogist, 1977. V. 62. P. 351 -355.

Vergasova L.P., Krivovichev S.V., Britvin S.N., Burns C.P., Ananiev V.V. Filatovite, K[(Al,Zn)2(As,Si)2O8], a new mineral species from the Tolbachik volcano, Kamchatka peninsula, Russia. Eur. J. Mineral. 2004. V. 16. P. 533-536.

## Kovalskaya T.N., Khanin D.A., Varlamov D.A., Kalinin G.M. Allanite synthesis in hydrothermal conditions. Preliminary data.

Institute of Experimental Mineralogy Russian Academy of Sciences tatiana76@iem.ac.ru

**Abstract:** This work is devoted to the experimental study of the formation of allanite in hydrothermal conditions and isomorphic substitution $Ca^{2+}\leftrightarrow Ce^{3+}$, $Si^{4+}\leftrightarrow Al^{3+}$, $Ca^{2+}\leftrightarrow Y^{3+}$, $Fe^{3+}\leftrightarrow Ce^{3+}$ and $Fe^{3+}\leftrightarrow Y^{3+}$ in it. Conducted 2 series of experiments on the synthesis at a temperature of 500-550 $^{o}$C and a pressure of 4 kbar. Various silicate cerium and yttrium phases, including the epidote composition, were obtained in the products.

***Keywords**: epidote, allanite, hydrothermal conditions, experiment, cerium, ittrium, isomorphic substitution, allanite-(Ce), allanite-(Y)*

Minerals of the epidote group are widespread rock-forming and accessory minerals in many types of metamosotic rocks, as well as in a number of igneous and metamorphic rocks (Varlamov et al., 2019). They are a kind of indicators of geochemical processes that occur during the formation and change of a particular rock. The initial interest was caused by the discovery during the field work at the Tykotlov ore occurrence (Polar Urals) of samples of gallium containing allanite (Ce), in intergrowth with Ga epidote (Varlamov et al., 2011). Their joint finding and accretion indicates their simultaneous formation (Kovalskaya et al., 2019), and the unevenness in the redistribution of cerium and gallium on the unusual conditions of their formation. The authors carried out a series of experiments on the synthesis of Ga - epidote in a wide range of compositions at temperatures up to 500 °C and pressures up to 5 kbar. In order to recreate the conditions of formation of the allanite - (Ce) - epidote - (Ga) association and assess the distribution of components, in this work, attempts were made to synthesize allanite under similar conditions. For this purpose, steichometric helium mixtures of allanites of different composition - allanite- (Ce) and allanite- (Y) were prepared. Then the mixture was loaded into platinum ampoules with a diameter of 4-5 mm in the ratio of fluid / sample 1/10. Distilled water was used as a fluid. The experiments were carried out on a high-pressure gas installation with internal heating (UVGD-10000) at a temperature of 500 and 550 ° C and a pressure of 4-5 kbar. The only difference was that before holding at 500 °C and 550 °C and a pressure of 4 kbar, the reaction mixture was kept for 3 hours at a temperature of 1100 ° C and a pressure of 4 kbar. It was necessary to homogenize the mixture. Then, isobaric cooling to 500°C occurred. The duration of the experiments was 10 days.

As a result of the experiments, small intergrowths up to 50 μm, composed of split crystals of cerium-containing epidote, were obtained (Fig. 1).

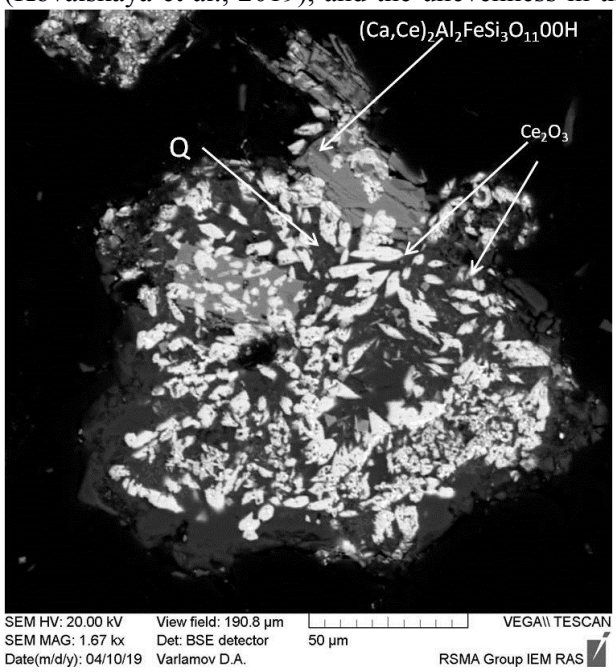


**Fig. 1.** Crystals of synthesized cerium epidote.

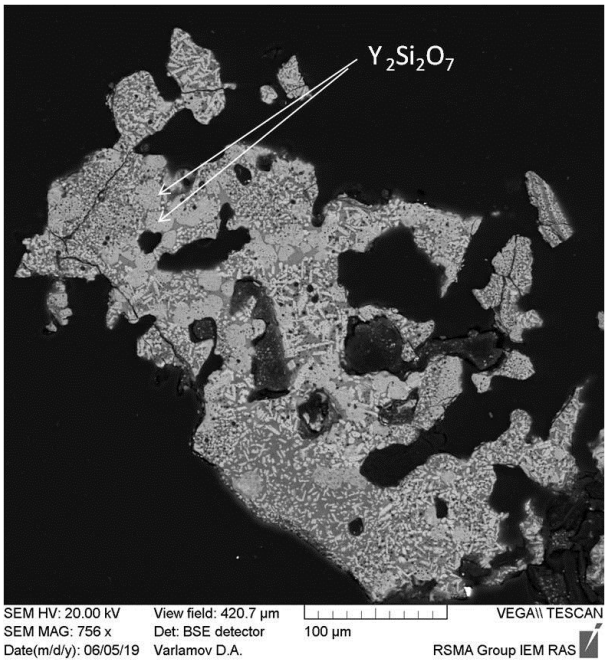


**Fig. 2.** Crystals of synthetic yttrialite.

These crystals partially grow together with quartz and $Ce_2O_3$; this experiment was carried out with the complete replacement of $Ca^{2+}\leftrightarrow Ce^{3+}$. The first series of experiments was carried out at a temperature of 550°C and a pressure of 5 kbar. Allanite disintegration similar to the epidote-Ga disintegration described in Kovalskaya et al. (2015) occurred in the products of these experiments. As a result, the formation of a phase with a stoichiometry of the composition corresponding to the formula $Ca_2Ce_2Si_2O_8$ and the phase $Ca_3Ce^{3+}{}_2[SiO_4]_3$,

corresponding in composition to the garnet was observed.

At a temperature of 500°C, the cerium is partially filled with position A, instead of Al. The content of $Ce_2O_3$ in this case reaches 8.6 wt.%, And $Al_2O_3$ - 33.2 wt.%. In general, at fairly low temperatures, calcium is almost completely replaced by cerium, as well as partial replacement of aluminum. With an even greater decrease in temperature, only calcium is replaced by cerium, as well as silicon by aluminum to compensate for the charges. At temperatures above 550 °C, a more stable anortite-like cerium phase is formed instead of epidote. In experiments with the replacement of $Ca^{2+} \leftrightarrow Y^{3+}$ at 500 ° C and a pressure of 4 kbar, the most stable phase is yttrialite of composition $Y_2Si_2O_7$ (Fig. 2). The obtained data indicate that, at given P-T parameters, cerium and yttrium silicates are stable, however, such conditions are not sufficient for the formation of allanites as the main phase. In some experiments at a temperature of 500°C, phases similar to allanites by stoichiometry were obtained, but most likely they are the final phases of crystallization. Work on the synthesis and study of allatites, as well as other phases in the system Ca-Ce-Y-Fe-Al-Si-O-$H_2O$ will be continued.

**References:**


Varlamov D.A., Ermolaeva V.N., Chukanov N.V., Yanchev S., Vigasina M.F., Plechov P.Yu. (2019) New data on the chemical composition and Raman spectra of the minerals of the epidote supergroup. ZRMO, 1, 79-99 (in Russian)

Kovalskaya, TN, Varlamov, D. A., Kotelnikov, A. R., Kalinin, G. M. The possibility of gallium being incorporated into the structure of silicates and aluminosilicates. In Reports of the VIII International Symposium "Mineral Diversity - Research and Conservation" (2015), National Museum of the Land and People of Sofia, pp. 142–145. (in Russian)

Kovalskaya T.N., Varlamov D.A., Kotelnikov A.R., Chukanov N.V., Kalinin G.M. (2019) Hydrothermal synthesis of gallium epidote - an analogue of the phase Ca2Al2Ga (Si3O12) (OH) from Tykotlovsk gold-sulphide manifestation. Geochemistry, 10, in print. (in Russian)

Varlamov D., Soboleva A., Mayorova T., Kotelnikov A., Kovalskaya T. (2011) Abstr. of vi int. symposium "Mineral diversity - research and preservation", Sofia, Bulgaria, Earth and Man National Museum, 22


## Nesterova V.A.[1,2], Setkova T.V.[2], Pushcharovsky D.Yu.[1], Balitsky V.S.[2], Borovikova E.Y.[1], Nekrasov A.N.[2], Bublikova T.M.[2], Kvas P.S.[1,2] Hydrothermal synthesis of gallium-, germanium bearing tourmaline's analogue.UDC 549.612


[1]Department of Geology, Lomonosov MSU, Moscow, [2]IEM RAS, Chernogolovka (v_nest.243@mail.ru)



**Abstract.** (Ga, Ge)-bearing tourmaline was synthesized in hydrothermal condition at temperature 600-650 °C and pressure of 100 MPa in solutions of boric acid on elbaite seed. The newly formed layer of tourmaline reaches a thickness of 50-100 microns in a direction of the third order axis. The content of $Ga_2O_3$ and $GeO_2$ is about 20 and 2 wt. % respectively. EMPA – analysis detected uniform gallium and germanium spreading. Raman spectroscopy confirmed the identity of the overgrown layer to the mineralogical group of tourmaline.



***Keywords:*** *tourmaline, crystal growth, hydrothermal synthesis, gallium, germanium, aluminosilicate, borosilicate, Raman spectroscopy.*


**Introduction.** It is known that tourmaline is widely used in radio engineering because of its pyro and piezoelectric properties, as well as in in the jewelry industry due to great variety of its color. Since today, it was not possible to obtain synthetic crystals of tourmaline of sufficient size. Mainly natural samples of tourmaline are used for industrial purposes. Therefore, researches related to tourmaline's growth are very important nowadays. At the end of 2018 it was established (O'bannon et al., 2018) that the space group of tourmaline is R3m in crystals, subjected to pressure of 15.4 GPa, may be replaced by R3, first of all, due to distortion of silica oxide $T_6O_{18}$ rings. By the example of a large group of minerals and synthetic crystals it was shown that changes in their structures under the influence of high pressures can be simulated chemically by introducing larger cations into their structure. In this case, ion radii ratio of the cation/anion will increase, and corresponding chemical deformations in structure can be considered similar to the high-pressure one. It is known that gallium and germanium in chemical properties are similar to aluminum and silicon respectively, but the ions size of $Ga^{3+}$ and $Ge^{4+}$ is more ($r Ge^{4+}/r Si^{4+}$=2.04; $r Ga^{3+}/r Al^{3+}$=1.17). In this regard, synthesis of tourmaline crystals in which gallium and germanium will isomorphically replace aluminum and silicon is of considerable interest. In addition to comparing structural characteristics of such crystals with the structural changes of tourmaline under high pressure, it can be assumed such crystals will have more pronounced pyro-and piezoelectric properties. Previously similar effect was already established by the example of Ge-rich quartz crystals (Balitsky et al., 2017).

**Experimental methods.** Crystal growth of Ga- and Ge-bearing tourmaline was performed in thermogradient hydrothermal conditions at a temperature of 600-650 °C and a pressure of 100 MPa in autoclaves made of Cr-Ni alloy. The previously developed method of tourmaline growth on seed was taken as a basis (Setkova et al., 2009; Setkova et al. 2011; Vereshchagin et al. 2016). Mixture of synthetic quartz and corundum fragments with additives of gallium and germanium oxide

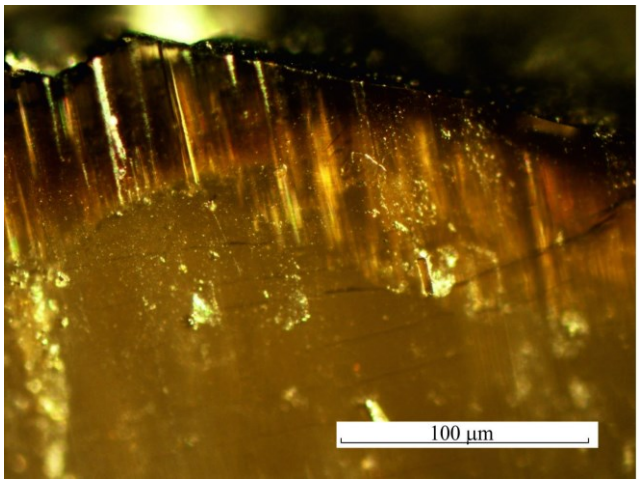


**Fig. 1.** Overgrown layer of Ga, Ge-containing tourmaline (Nikon Eclipse lv100PO L microscope)

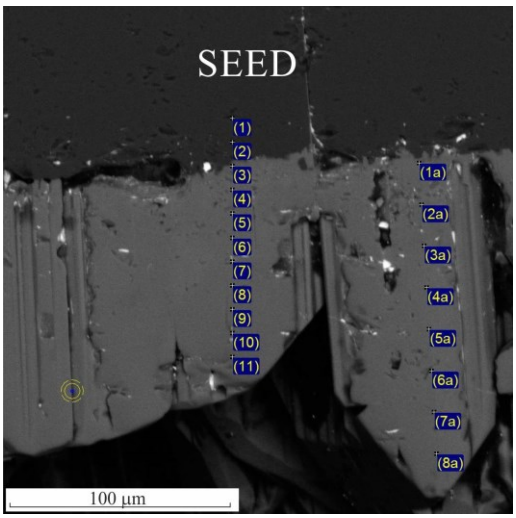


**Fig. 2** SEM image of Ga, Ge-containing tourmaline (light gray), formed on elbaite seed (dark gray). The points marked in the figure were used to obtain average data on the chemical composition.

powders was used as a nutrient material. Seeds were an elbaite crystals selected from pegmatites Malkhan Deposit (Transbaikalia). Autoclaves loaded with nutrient and seeds were filled with boric acid solution (20 wt.% $H_3BO_3$). Pressure was set by the autoclave filling factor (Naumov et al., 1971). The duration of the experiments was 20 days. The experimental products and seed crystals were studied under optical (MBS-10), polarization (Nikon Eclipse LV100pol) and electronic scanning (Tescan Vega II XMU) microscopes. The composition of the newly formed phases was analyzed by electron probe microanalysis (Tescan Vega II XMU). Identification of the overgrown layer was carried out by Raman spectra (JY Horiba XPloRA) taking into account the data of electron probe microanalysis.

**Table 1.** The chemical composition of the overgrown layer and the estimated distribution of elements in crystal-chemical positions.

| Oxide | Mean wt. % |
|---|---|
| | |
| $Na_2O$ | 1.64 |
| $Al_2O_3$ | 21.62 |
| $SiO_2$ | 27.73 |
| CaO | 0.25 |
| $TiO_2$ | 0.63 |
| $Cr_2O_3$ | 0.02 |
| FeO | 9.49 |
| NiO | 0.13 |
| $Ga_2O_3$ | 20.77 |
| $GeO_2$ | 1.63 |
| Sum | 83.95 |
| $\Sigma B_2O_3$, $H_2O$ | 16.05 |

| Position | Element | Formula unit |
|---|---|---|
| *T* | Si | 5.40 |
| | Ge | 0.14 |
| | Al | 0.46 |
| | Total | **6** |
| *Y+Z* | Al | 4.67 |
| | Ga | 2.62 |
| | Fe | 1.59 |
| | Ti | 0.10 |
| | Ni | 0.02 |
| | Total | **9** |
| *X* | Na | 0.56 |
| | Ca | 0.06 |
| | Total | 0.62 |
| *V+W* | O | 0.71 |
| | OH | 3.29 |
| | Total | **4** |

$^{X}(\square_{0.38}Na_{0.56}Ca_{0.06})^{Y+Z}(Fe_{1.59}Ga_{2.62}Al_{4.67}Ni_{0.02}Ti_{0.10})^{T}(Si_{5.40}Ge_{0.14}Al_{0.46})O_{18}(BO_3)_3(OH_{3.29}O_{0.71})$*

* Y and Z positions are not separated due to the lack of X-ray structural data.

**Results.** As a result of experiments, on elbaite seed was obtained outgrowth 50-100 microns thick

(fig. 1) dark brown, almost black in color. The overgrown layer is formed on the surface of the pinacoid face {0001}, characterized by a rough surface and is composed of a set of faces of trigonal pyramids {1011} formed along the main crystallographic direction of tourmaline (L3 axis). On the {0001} face of the newly formed layer is absent, which may be consequence of the very low growth rate of tourmaline in this direction. The content of gallium and germanium in the newly formed layer is 20 wt. % $Ga_2O_3$ and 2 wt. % $GeO_2$, respectively (table 1), and the distribution of these elements in the overgrown layer is uniform (fig.2). Overgrown layer has an increased iron content (9.5 wt. % FeO), titanium (0.63 wt.% $TiO_2$) and lowed silicon (27.7 wt. % $SiO_2$) and aluminum (21.6 wt. % $Al_2O_3$) content compared with the seed crystal. Belonging of the overgrown layer to the tourmaline group was confirmed by comparison of its Raman spectrum with the spectra of natural tourmaline (Watenphul et al., 2016). Since the structure of the newly formed tourmaline is composed of heavier cations Ga and Ge, a shift of the spectrum bands to smaller frequencies present compared to spectrum bands of seed of elbaite.

Based on the data of electron probe microanalysis, an approximate crystal chemical formula of the newly formed (Ga, Ge)-bearing tourmaline was estimated (see table 2). The formula was calculated based on the setup: the sum of the cations in *T*-, *Y*-, and *Z*- positions is equal to 15. Valences were compensated by the ratio of $O^{2-}$ and $OH^-$ in *U* and *W* positions.

**Conclusions.** Thus, the possibility of crystal growth of (Ga, Ge)-bearing tourmaline in hydrothermal conditions at a temperature of 600-650°C and a pressure of 100 MPa in solutions of boric acid on elbaite seed was experimentally shown. The overgrown layer of (Ga, Ge)-bearing tourmaline in the pinacoid direction reaches a thickness of 50-100 microns; its content of $Ga_2O_3$ and $GeO_2$ is about 20 and 2 wt. % respectively. The distribution of gallium and germanium impurities in the overgrown layer is uniform. Further research should focus on increasing the thickness of the overgrown layer and the proportion of gallium and germanium impurities in the grown crystals.

**Acknowledgments.** The reported study was funded by RFBR, project number 17-05-00976 and 18-05-00332.

**References:**

Balitsky V. S., Balitsky D. V., Pushcharovsky D. Yu., Balitskaya L. V., Setkova T. V., and Dokina T. N. (2019) Epitaxial growth, morphology, and temperature stability of quartz-like germanium dioxide crystals Doklady Earth Sciences. 485, 1, 264–267.

O'Bannon E., Beavers C., Kuntz M., Williams Q. High-pressure study of dravite tourmaline: Insights into the accommodating nature of the tourmaline structure // American mineralogist, 2018, V. 103. P. 1622-1633.

Setkova T., Shapovalov Yu., Balitsky V. Growth of tourmaline single crystals containing transition metal elements in hydrothermal solutions // Journal of Crystal Growth. 2011. V.318, P. 904–907.

Setkova T.V., Shapovalov Yu.B., and Balitskii V.S. (2009) Experimental growth and structural-morphological characteristics of co-tourmaline. Doklady Earth Sciences, 424, 1, 82–85.

Vereshchagin O.S., Setkova T.V., Rozhdestvenskaya I.V., Frank-Kamenetskaya O.V., Deyneko D.V., Pokholok K.V. Synthesis and crystal structure of Ga, Fe-bearing tourmaline. European Journal of Mineralogy, 2016, V.28, 3, p. 593–599.

Watenphul A., Burgdorf M., Schlüter J., Horn I., Malcherek T., Mihailova B. Exploring the potential of Raman spectroscopy for crystallochemical analyses of complex hydrous silicates: II. Tourmalines // American Mineralogist, 2016, V. 101, P. 970–985.

## Reutova O.V.[1], Redkin A.F.[2] Structural transformations in compounds of $Ca_{2-x}Cd_xSb_2O_7$ composition, obtained by hydrothermal synthesis

[1] Faculty of Geology MSU, Moscow (reutova.olia@yandex.ru); [2] IEM RAS, Chernogolovka (redkin@iem.ac.ru)

**Abstract.** The effect of the ratio of $Ca^{2+}$ and $Cd^{2+}$ in the compounds of $Ca_{2-x}Cd_xSb_2O_7$ on the structure of synthesis products at 700-800 °C and 1.6-2 kbar in water is studied. It was shown that the introduction of a significant amount of $Ca^{2+}$ into the compound causes structural transformations of $Fd\bar{3}m$ (cub. sing.)→ *Imma* (orthorhombic sing.). The influence of the mole fraction of $Ca^{2+}$ on the parameter of the unit cell of pyrochlore (rometite) is considered

***Keywords:*** *hydrothermal synthesis, pyrochlore, romeite, weberite, crystal structure*

Synthesis of minerals with a given chemical composition, structure and of cell parameters (CP) is a pressing task. Of particular interest are pyrochlores - oxide compounds of the $A_2B_2O_6(O,OH,F)$ composition, having a structure $Fd\bar{3}m$ which find wide use as catalysts in organic synthesis, and their electrical and optical properties are in demand in the electronic industry. Isomorphic substitution of cations can also serve as an indicator of the formation conditions of these minerals under natural conditions. Pyrochlores belonging to the rometite subgroup containing antimony (V) in position $^{[6]}B$ are rarely found in nature, but many researchers show considerable interest in them.

Preferable synthesis of of romeite of compositions $Ca_{2-x}Me_xSb_2O_7$, where Me – $Mg^{2+}$, $Cd^{2+}$, $Pb^{2+}$, etc. was a method of dry synthesis at high temperature (up to 1300 °C). The mixtures based on Sb(III) oxide were used as the starting charge, which during the multi-stage experiment was to be oxidized with air oxygen to the Sb(V) state. Compounds of composition $Ca_2Sb_2O_7$, $Cd_2Sb_2O_7$, $Sr_2Sb_2O_7$ (Byström, 1944), $Pb_2Sb_2O_7$ (Au et al., 2007) were found to crystallize in a structural type of weberite. It is noted (Au et al., 2007) that pressure increase contributes to the formation of pyrochlore structure $Ca_2Sb_2O_7$ instead of weberite, whereas temperature rise stabilizes weberite structure.

The addition of fluorine to complex oxide compounds Sb(V) stabilizes the structural type of romeite. However, the composition of romeite, according to studies (Aia et al., 1963), differs from ideal and it characterized by calcium deficiency. CP ($Ca_xCd_{1-x}$), ($Ca_xMn_{1-x}$), ($Mn_xCd_{1-x}$) solid solutions of romeites have linear dependence on molar fraction of cation (x) in position [8]A.

Synthesis of crystals was carried out in high-pressure hydrothermal line. Mixtures corresponding to the stoichiometry of the compounds were prepared from the starting pure chemicals CaO, CdO and $Sb_2O_5$. Experiments were carried out in Pt ampoules and distilled water. Earlier (Redkin et al., 2013), it was found that in order to preserve Sb(V), it is necessary to reduce the synthesis time at 800 ° C, 2 kbar to 12-24 hours. The parameters of the experiments and the composition of the starting mixtures were as follows:

| 800°C, 2.0 Kb (12, 24 hours) | 700°C, 1.6 Kb (48 hours) |
|---|---|
| $Cd_2Sb_2O_7$ | |
| $Ca_{0.5}Cd_{1.5}Sb_2O_7$ | |
| $Ca_{1.0}Cd_{1.0}Sb_2O_7$ | $Ca_{1.0}Cd_{1.0}Sb_2O_7$ |
| $Ca_{1.5}Cd_{0.5}Sb_2O_7$ | $Ca_{1.5}Cd_{0.5}Sb_2O_7$ |
| $Ca_2Sb_2O_7$ | $Ca_2Sb_2O_7$ |

The products of the experiments were thoroughly washed from water-soluble compounds and investigated by XRD, XPS and SEM. All the compositions of the mixtures selected for the experiments were in the stability region of pyrochlore

As a result, finely crystalline (2–10 μm) homogeneous phases were obtained (Fig. 1 a, b, c), the X-ray diffraction patterns of which corresponded to romeite, weberite and their mixtures (Fig. 2, 3).

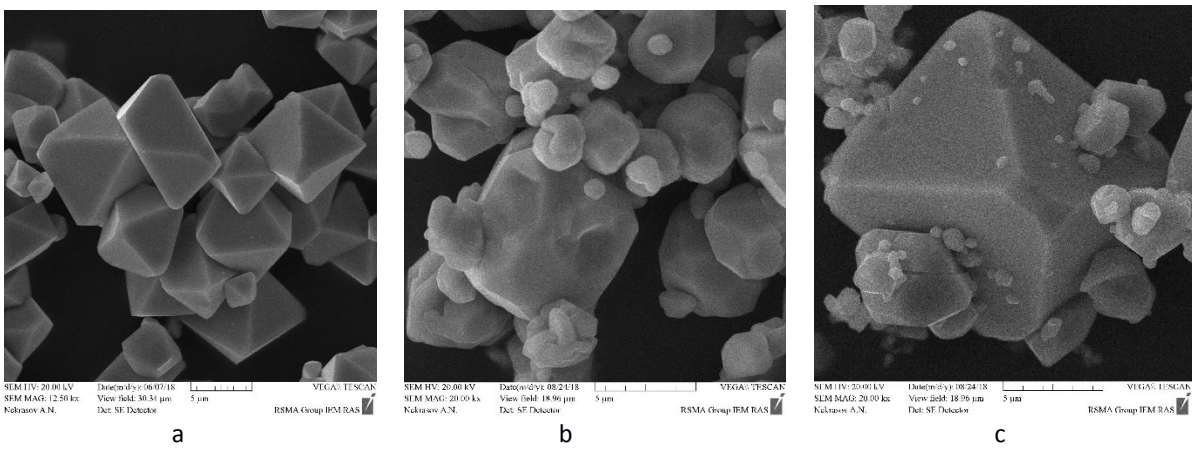


**Fig. 1.** SEM photo of the run products at 800 ° C, 2 Kb from the mixtures of composition $Cd_2Sb_2O_7$ (a), $Ca_{1.5}Cd_{0.5}Sb_2O_7$ (b), $Ca_2Sb_2O_7$ (c).

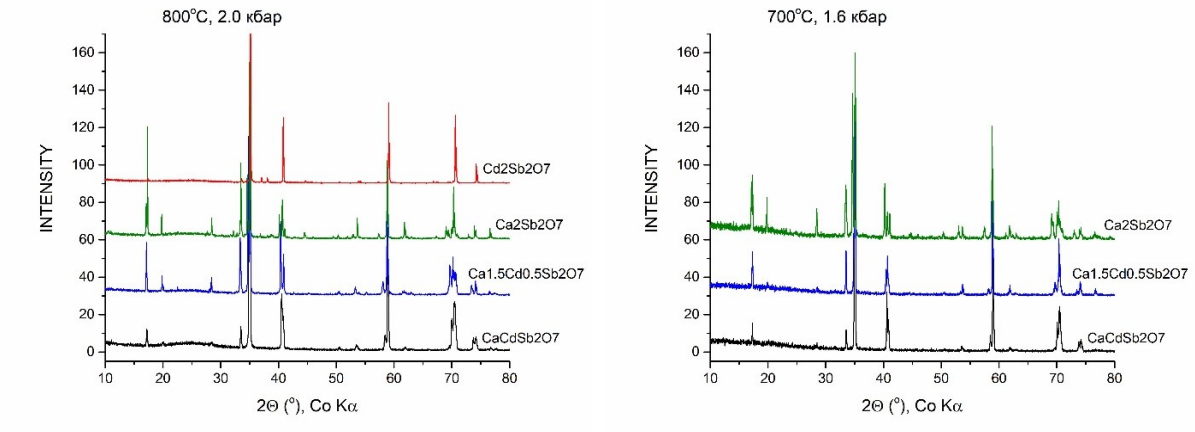


**Fig. 2.** X-ray diffraction patterns (XRD) of the run products at 800 ° C, 2 Kb.

**Fig. 3.** XRD of the run products at 700 ° C, 1.6 Kb.

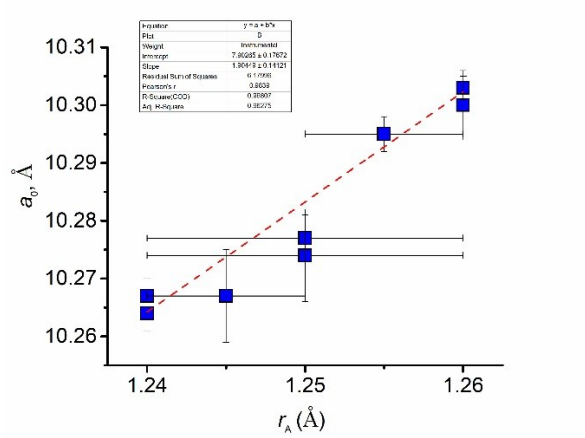


**Fig. 4.** Dependence of the CP (Ca-Cd) -romeites on the effective radius of the cation at the position [8]A.

$Cd_2Sb_2O_7$ romeite (Fig. 1-a) was pale green in color, and all other compounds containing $Ca^{2+}$ were white. Based on the data of the X-ray diffraction patterns, the CP of all the compounds obtained were calculated. The CP data of pyrochlore of the romeite group correlate with the ionic radii of cations at position [8]A (Fig. 4): for $Ca^{2+}$ $r$=1.26 Å, for $Cd^{2+}$ $r$=1.24 Å (Shannon, 1976).

X-ray photoelectron spectroscopy (XPS) was used to study the antimony state in the romeite of the $CaCdSb_2O_7$ composition. It was found that the characteristic binding energies of Sb 3d5/2, Sb 3d3/2 of compounds $Sb_2O_3$, $Sb_2O_4$, $Sb_2O_5$ and O 1s of the oxygen anion and (or) oxygen adsorbed compounds have close values (Garbassi, 1980), so that the decomposition of the spectrum into components is impossible.

Cell parameters ($a_0$, $b_0$, $c_0$) of weberites of composition $Ca_2Sb_2O_7$ and their comparison with published data are presented in Table 1.

**Table 1.** CP of weberites (space group: *Imma*) $Ca_2Sb_2O_7$ .

| | $a_0$ | $b_0$ | $c_0$ |
|---|---|---|---|
| Byström, 1944 | 7.28 | 7.44 | 10.18 |
| Ivanov et al., 1998 | 7.306 | 10.2263 | 7.4627 |
| Sato et al., 2002 | 7.29 | 10.2 | 7.45 |
| Au et.al., 2007 | 7.301 | 10.215 | 7.466 |
| Lin et al., 2006 | 7.29 | 10.2 | 7.45 |
| Chelazzi et al., $2011_1$ | 7.2947(1) | 10.2149(3) | 7.4502(2) |
| Chelazzi et al., $2011_2$ | 7.3043(2) | 10.2253(4) | 7.4611(2) |
| Chelazzi et al., $2011_3$ | 7.2818(4) | 10.1839(5) | 7.4467(4) |
| Basuev et al., 2013 | 7.294(0.3) | 10.216(0.4) | 7.448(3) |
| Our exp. (24 h, 800 °C, 2 Kb) | 7.284 | 10.307 | 7.458 |
| Our exp. (12 h, 800°C, 2 Kb) | 7.284 | 10.296 | 7.433 |
| Our exp. (48ч, 800 °C, 1.6 Kb) | 7.284 | 10.267 | 7.436 |

It follows from the table that the CP of weberites depends on the synthesis conditions and, apparently, on the $Sb^{5+}/Sb^{3+}$ ratio in them. According to modern concepts (Cai & Nino, 2009), orthorhombic weberite is assigned to the *Imma* structural group (No.74).

Studies have shown that oxide romeites containing $Ca^{2+}$ are not stable at 800 ° C and 2 Kb and turn into weberites. We assume that the stability region of Ca-Cd romeites is located at lower temperatures and, or, salt solutions that create an alkaline environment are necessary. However, it is known (ITC, 2004) that there is no direct transition $Fd\bar{3}m$ → *Imma* between the structural types of romeite and weberite. Such a unit cell transformation is possible according to the scheme:

**Romeite**: Cubic $Fd\bar{3}m$ ($O_h$) $a = b = c$, $\alpha=\beta=\gamma=90°$

↓

**?** Tetragonal $I4_1/a$ ($C_{4h}$) $a = b \neq c$, $\alpha=\beta=\gamma=90°$

↓

**Weberite**: Rhombic *Imma* ($D_{2h}$) $a \neq b \neq c$, $\alpha=\beta=\gamma=90°$

Thus, it has been established that romeites containing significant amounts of $Ca^{2+}$ are not stable and turn into weberites (orthorhombic syngony, *Imma* SG). The main reason limiting the stability of the pyrochlore structure is apparently the instability of $Sb^{5+}$ in the octahedral position [6]B.

***Acknowledgments*** This research was supported from the Grants of Russian Foundation for the Basic Research and project No AAAA-A18-118020590150-6 of the IEM RAS. The authors are grateful to A.N. Nekrasov, T.N. Dokina and O.L. Samokhvalova (all from IEM RAS) for their help in analyzing the products of experiments on a scanning electron microscope and on an X-ray diffractometer, prof., Dr. Sc. A.M. Ionov and R.N. Mozhchil (both from IFTT RAS) for XPS research.

**References:**

Aia M.A., Mooney R.W., and Hoffman C.W.W. (1963). An X-Ray Study of Pyrochlore Fluoantimonates of

Calcium, Cadmium, and Manganese. J Electrochem Soc 110 [10] 1048-1054.

Au Y.S., Fu W.T., Ijdo D.J.W. (2007). Crystal structure of $Ca_2Ln_3Sb_3O_{14}$ (*Ln* = La, Pr, Nd and Y): A novel variant of weberite. J Solid State Chem 180 3166–3171

Bazuev G.V., Tyutyunnik A.P., and Golovkin B.G. (2013). Phase Chemistry in the Ca-Mn-Sb-O System at 1160–1250 °C. Z. Anorg Allg Chem 639 [14] 2657–2663

Byström A. (1944). X-Ray analysis of $Ca_2Sb_2O_7$ and compounds of similar composition, Arkiv for kemi, mineralogi och geologi 21 (Band 18 A) 1-8.

Cai L. and Nino J.C. (2009). Complex Ceramic Structures. I. Weberites. Acta Cryst B65 269-290.

Chelazzi L, Ballaran TB, Bindi L, Bonazzi P. (2011). In situ high-temperature X-ray powder diffraction study of the synthetic $Ca_2Sb_2O_7$ weberite-type compound. *Period Mineral* 80: 145-153.

Chelazzi L, Boffa Ballaran T, Nestola F, Bindi L, Bonazzi P. (2011). High-pressure behavior of the synthetic $Ca_2Sb_2O_7$ weberite-type compound. *Solid State Sci* 13: 1092-1095.

Garbassi F. (1980). XPS and AES study of antimony oxides. Surf Interface Anal 2 165-169.

*ITS* (*2004). International Tables for Crystallography* Volume *A1*. Symmetry relations between space groups. (Editors: H. Wondratschek & U. Müller) 399.

Ivanov S., Tellgren R., and Rundlof H. (1998). Structural aspects of ferroelectric phase transitions in complex metal oxides $A_2Sb_2O_7$ (A = Pb, Sr, Ca) with Weberite Structure. European Powder Diffraction Conference 5, Pts 1 Materials Science Forum 278-281 768-772.

Lin X., Huang F., Wang W., Wang Y., Xia Y., Shi J. (2006). Photocatalytic activities of $M_2Sb_2O_7$ (M = Ca, Sr) for degrading methyl orange. Appl Catal A: General 313 218–223

Redkin A.F., Ionov A.M., and Kotova N.P. (2013). Hydrothermal synthesis of pyrochlores and their characterization. Phys Chem Minerals 40 733–745.

Shannon R.D. (1976). Revised effective ionic radii and systematic studies of interatomic distances in halides and chalcogenides. Acta Cryst A32 751-767.

Sato J., Saito N., Nishiyama H., and Inoue Y. (2002). Photocatalytic water decomposition by $RuO_2$-loaded antimonates, $M_2Sb_2O_7$ (M = Ca, Sr), $CaSb_2O_6$ and $NaSbO_3$, with $d^{10}$ configuration. J Photoch Photobio A: Chemistry 148 85–89.